Frequency Modelling and Solution of Fluid-Structure Interaction in Complex Pipelines

Yuanzhi Xu[1,2]
D. Nigel Johnston[2]
Zongxia Jiao[1] (corresponding author: zxjiao@buaa.edu.cn)
Andrew R. Plummer[2]

1. School of Automation Science and Electrical Engineering, Beihang University
No.37, Xueyuan Road, Haidian District, Beijing, China, 100191
2. Department of Mechanical Engineering, University of Bath
University of Bath, Bath, UK, BA2 7AY

Abstract

Complex pipelines may have various structural supports and boundary conditions, as well as branches. To analyse the vibrational characteristics of piping systems, frequency modelling and solution methods considering complex constraints are developed here. A fourteen-equation model and Transfer Matrix Method (TMM) are employed to describe Fluid-Structure Interaction (FSI) in liquid-filled pipes. A general solution for the multi-branch pipe is proposed in this paper, offering a methodology to predict frequency responses of the complex piping system. Some branched pipe systems are built for the purpose of validation, indicating good agreement with calculated results.

Keywords: Fluid-structure interaction; pipeline; vibration

Nomenclature

Uppercase Letters

A	cross-sectional area
E	Young's modulus
F	external force of constraints
G	shear modulus
I	flexure moment of inertia
J	polar moment of inertia
K	fluid bulk modulus
L	length of pipe
P	fluid pressure
T	external moment of constraints
V	fluid velocity
Y	angular impedance of constraints
Z	linear impedance of constraints

Lowercase Letters

c	wave speed
e	thickness of pipe wall
f	force in cross-section
m	pipe moment or extra mass of constraints
r	radii of pipe cross-section
u	pipe displacement
z	distance along the pipe
ρ	density
ν	Poisson's ratio
ψ	pipe rotation displacement
φ	angle between two adjacent coordinate systems

Subscripts

e	external excitation
f	fluid
p	pipe
i	inner
o	outer
x, y	lateral coordinates
z	axial coordinate

Superscripts

$\sim$	Laplace transformed
T	transposed

Matrices and Vectors

$\mathbf{A}$, $\mathbf{B}$, $\mathbf{C}$	coefficient matrix of FSI model
$\mathbf{D}$	boundary matrix
$\mathbf{I}$	identity matrix
$\mathbf{M}$	field transfer matrix
$\mathbf{N}$	constraint matrix
$\mathbf{Q}$	excitation vector
$\mathbf{R}$	rotation matrix
$\mathbf{T}$	point transfer matrix of T-junction
$\boldsymbol{\phi}$	state vector of 14 variables
$\mathbf{0}$	zero vector/matrix

1. Introduction

Fluid-Structure Interaction (FSI) describes an explicit coupling between moving fluid and deformable structure, in which fluid acts on the structure with fluidic force whilst simultaneously the fluid is acted upon by movement of the structural boundary. The FSI in a fluid-conveying pipeline can be induced by sudden opening or closing of a valve, sudden start-up or shutdown of a pump, fluid flow ripples and mechanical excitation. This phenomenon has been found in a wide range of fields, ranging from hydraulic and pneumatic fluid power systems, water supply systems, power production, petrochemical industry, and even biological vessels. This paper is focused on the FSI in liquid-filled pipes, especially applied to hydraulic piping systems of complex supports and spatial configurations.

Structural supports will affect the behaviour of a piping system significantly, changing the system's natural frequencies. In this paper, various boundary conditions and middle constraints are studied and included in the pipe system model. Although models of straight, curved and T-shaped pipes have been studied previously, a more complicated system has not yet been intensively researched. In the present work, a general solution of the multi-branch pipe system is proposed, and experiments are carried out.

1.1. Literature of analytical model

Water hammer theory was developed in the 19th century, mostly based on the research of Joukowsky [1], who presented the formula to predict the pressure change ΔP with the velocity change ΔV,

$$\Delta P = \rho_f c_f \Delta V \,. \tag{1}$$

Although Joukowsky used the sound velocity which takes into account both the compressibility of the fluid and the elasticity of the pipe walls [2], the expression was a one-way coupling excluding structural vibration. Wylie & Streeter [3] and Cai [4] presented the impedance method, and the pipe elasticity was incorporated. It was simple and effective in predicting behaviours of fluid transients, but still not in a coupled way.

The two-way coupling mechanism between the fluid transient and the movement of pipe wall has been defined as three kinds of coupling [2,5,6]. *Poisson coupling* is due to the Poisson effect, in which an oscillatory pressure force results in radial pipe wall dilation and hence axial strain and movement. J*unction coupling* takes place at changed boundaries, such as elbows, valves, junctions and pipe ends due to the unbalanced pressure force acting on an area. *Friction coupling* is due to shear stresses on pipe walls, and is generally considered less significant than the other two couplings.

Basic water hammer equations (two-equation model [2]) could be derived from the Navier-Stokes equation and the continuity equation (Zielke [7]),

$$\frac{\partial V}{\partial t}+\frac{1}{\rho_f}\frac{\partial P}{\partial z}=0, \tag{2}$$

$$\frac{\partial V}{\partial z}+\frac{1}{K}\frac{\partial P}{\partial t}=0. \tag{3}$$

Skalak [8,9] later proposed four linear first-order partial differential equations (PDEs) for the two-way interaction, which was also known as the four-equation model. Wiggert *et al*. [10] presented an axial four-equation model containing the Poisson coupling, based on the work of Walker and Phillips [11]. The axial four-equation model was then widely used and achieved good predictions of straight pipes [12,13,14]. Zhang *et al*. [6] utilised the four-equation model to simulate the vibration of a liquid-filled straight pipe in the frequency domain. Eight equations for a curved pipe had been obtained by Davidson and Smith [15], extended by Valentin *et al*. [16] and Hu and Phillips [17], where Poisson and junction coupling were taken into account.

A fourteen element vector was first used by Davidson and Samsury [18] and applied on the simulation of a pipeline consisting of straight and curved pipes. Wilkinson [19] presented the 14-equation model where equations of motion were based on the Bernoulli-Euler beam theory. The linear fourteen-equation model then was extended and followed by Wiggert *et al*. [20] and many other researchers [21-30], including Poisson coupling and using Timoshenko-type beam theory. Lesmez [21,22] studied fourteen equations for a straight pipe and the transfer matrix of a bend, and more importantly included extra mass and the spring force in his model. Tentarelli [23] derived fourteen-equation models of straight and curved pipes, including friction coupling for the first time. Moreover, he also discussed the extra mass, springs and accumulators using linear lumped impedances, and considered various boundary conditions at pipe ends. The work of Tentarelli was perhaps the most significant and comprehensive for complex pipelines. El-Raheb [24] suggested a flexibility factor to modify the bending stiffness of curved pipes, which was followed by De Jong [25] who studied and tested FSI widely. Kwong and Edge [26,27] pointed out that as the pipe length increased the transfer matrix became ill-conditioned, and solved this problem by dividing the circuit into reasonably small sections. Then they optimized the fitness of the hydraulic circuit with the stiffness and location of clamps [28], which is a reliable and convenient modification for passive control of vibrations. Jiao *et al*. [29] added friction items into the fourteen-equation model, based on the work of Zielke [7]. Liu and Li [30] introduced the modelling of FSI in pipes with arbitrary elastic supports.

1.2. Literature of solution methods

The Transfer Matrix Method (TMM) has been used for analysing mechanical vibration since the 1960s [31], and was used by Davidson *et al*. [15,18] to solve a curved section successfully. The TMM was comprehensively introduced into the field of FSI in piping systems by Chaudhry [32], who defined the transfer matrix as a matrix relating two state vectors, and presented three types of them. The *field transfer matrix* relates state vectors at the two ends of a pipe section

(Fig.1(a))

$$\boldsymbol{\phi}_i^R = \mathbf{M}\boldsymbol{\phi}_i^L . \tag{4}$$

The *point transfer matrix* relates state vectors to the left and right of a discontinuity, such as a connection between two adjacent pipes of different radii, or a support in the middle of a pipeline (Fig.1(b))

$$\boldsymbol{\phi}_{i+1}^L = \mathbf{N}\boldsymbol{\phi}_i^R . \tag{5}$$

A junction, for example an elbow, can also be represented by a point transfer matrix by neglecting dimensions and dynamics of this section.

The *overall transfer matrix* (or global transfer matrix [21]) relates two ends of the entire piping system, which basically means a multiplication of intermediate field and point transfer matrices. Thus, models of all pipe sections, connections and junctions could be assembled and solved. TMM was systematically and extensively applied on one-dimensional, liquid-filled pipes [6,10,12,18 -30].

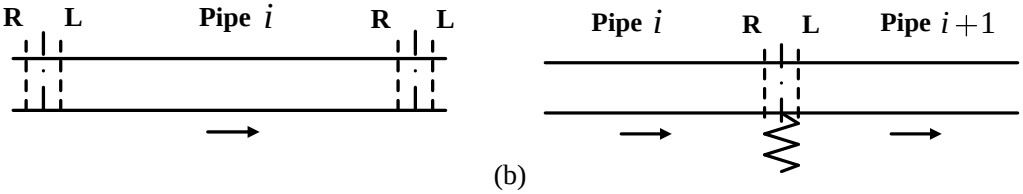

Fig.1 Transfer matrices of pipeline. (a) Field transfer matrix of pipe; (b) Point transfer matrix of series connection.

Solution methods in the time domain have been developed in a wide range of previous work. As the system of PDEs for FSI is actually a one-dimensional linear hyperbolic system with constant coefficients, it can be transformed into ordinary differential equations (ODEs) by the Method of Characteristics (MOC) [17,33,34,35]. This popular approach is to mesh the distance-time plane and time-march from initial conditions [5,13]. Wiggert *et al*. [10,20] used the MOC to solve pipelines containing elbows in the time domain and achieved good results. The 14-equation model and boundary conditions using the MOC are discussed by Tijsseling comprehensively [36]. Although linear models of FSI can be solved, the MOC is only suitable for constant properties. In reality properties could depend on time, frequency, pressure, temperature or flowrate, and the equations could be non-linear [37]. Other analytical solution methods in the time domain have been investigated, such as Glimm's method [37], MOC-FEM [38], and Godunov's method [39], extending from different solutions of hyperbolic PDEs. Another time domain solution named System Modal Approximation (SMA) [40] was developed to solve compound fluid-line systems, and achieved a good result.

The frequency domain solution of FSI in fluid-conveying pipes has been developed as an effective method. D'Souza and Oldenburger [41] applied Laplace transforms on the equations for axial vibration, and obtained frequency responses. Davidson *et al*. solved a curved pipe [15,18] using the TMM and exponential approach in the frequency domain, which then became a

widely used approach [19,21-28]. Nanayakkara and Perreira [42] applied wave theory and matrix exponential approach as solutions, and discussed the boundary and excitation conditions. Zhang and Tijsseling *et al*. [6] pointed out limitations of MOC and gave a solution based on Laplace transform with TMM, using the method of boundaries and excitation that Nanayakkara developed. Compared with results which were obtained by MOC and transformed into the frequency domain by Fast Fourier Transform (FFT), Zhang found the frequency method was more accurate and convenient. Liu and Li [30] also presented a frequency solution based on Laplace transforms, but this method was limited to straight pipes excluding curved sections [43]. Other methods to solve PDEs of FSI in the frequency domain have been investigated, such as wave approach [42] and Component Synthesis Method (CSM) [44].

1.3. Outline of paper

Although supports at intermediate positions as well as at pipe ends were studied by previous researchers [22,23,30], complex constraints including elasticity, damping and inertia have not been studied comprehensively. The first point of this paper (section 2) is focused on modelling of constraints relating to the 14-equation model, using the frequency domain method, which was developed by Zhang *et al*. [6], and TMM to model the whole system. Solution of a T-shaped pipe system is presented in section 3, and then extended to a multi-branch situation, forming a general solution for complex pipelines. The experiments for a T-shaped and a two-branch pipe system are mentioned in section 4, to prove the general solution method considering constraints of extra mass.

2. Modelling and solution of complex constraints

The fourteen-equation model describes the fluid behaviour and axial/flexural/torsional motions in 3-dimension space, basically containing two equations of fluid motion, and 6 sets of two equations describing each planar and rotational motion (Appendix A). The basic assumptions for the analytical model include: long wavelength relative to pipe diameter; low Mach numbers; absence of liquid column separation or air bubbles; linear elastic behaviour of piping material and fluid; and negligible inertia in the radial direction. Fluid friction is assumed to be negligible.

In this section, the frequency domain method mentioned by Zhang *et al*. [6] will be utilised to model FSI equations, and various fluid boundary conditions will be discussed as well. Complex constraints (including extra inertia, damping and elasticity) which may exist at both middle positions and pipe ends would be modelled and added into the global solution of the pipe system.

2.1. Frequency solution of FSI

Fourteen partial differential equations for a straight section are presented in Appendix A, and could be written [6] as

$$\mathbf{A}(\partial/\partial t)\boldsymbol{\phi}(z,t)+\mathbf{B}(\partial/\partial z)\boldsymbol{\phi}(z,t)+\mathbf{C}\boldsymbol{\phi}(z,t)=\mathbf{r}(z,t), \tag{6}$$

where $\boldsymbol{\phi}$ denotes the vector of system variables (velocity, pressure etc.), $\mathbf{A}$ and $\mathbf{B}$ are matrices of constant coefficients. $\mathbf{C}$ contains elements of friction and viscous damping, which is a constant matrix for laminar flow. The vector $\mathbf{r}$ describes the environmental source of excitation. The state vector at position z on the pipe is defined as a total of fourteen unknowns

$$\boldsymbol{\phi}(z,t)=\begin{matrix} V & P & \dot{u}_z & f_z & \dot{u}_y & f_y & \dot{\psi}_x & m_x & \dot{u}_x & f_x & \dot{\psi}_y & m_y & \dot{\psi}_z & m_z \end{matrix}^{\mathrm{T}}. \tag{7}$$

Then Eq.(6) can be Laplace transformed into the ordinary differential equation

$$\mathrm{s}\mathbf{A}^{*}(\mathrm{s})\tilde{\boldsymbol{\phi}}(z,\mathrm{s})+\mathbf{B}(\partial/\partial z)\tilde{\boldsymbol{\phi}}(z,\mathrm{s})=\tilde{\mathbf{r}}(z,\mathrm{s}), \tag{8}$$

in which symbols with $\sim$ denote transformed variables, and $\mathbf{A}^{*}(\mathrm{s})=\mathbf{A}+(1/\mathrm{s})\mathbf{C}$. For simplicity the values in the state vector can be defined relative to their mean or initial values, so the initial conditions can be eliminated.

Assuming that there is no spatially distributed excitation or initial disturbance, Ref. [6] obtained the relation between state vectors at two positions of pipeline,

$$\tilde{\boldsymbol{\phi}}(z,\mathrm{s})=\mathbf{M}(z,\mathrm{s})\tilde{\boldsymbol{\phi}}(0,\mathrm{s}), \tag{9}$$

where $\mathbf{M}(z,\mathrm{s})$ is defined as the field transfer matrix

$$\mathbf{M}(z,\mathrm{s})=\mathbf{S}(\mathrm{s})\mathbf{E}(z,\mathrm{s})\mathbf{S}^{-1}(\mathrm{s}). \tag{10}$$

Herein $\mathbf{S}$ consists of the eigenvectors of $\mathbf{A}^{*\text{-}1}\mathbf{B}$, and

$$\mathbf{E}(z,\mathrm{s})=\begin{pmatrix} \mathrm{e}^{-\mathrm{s}z/\lambda_1(\mathrm{s})} & & \\ & \mathrm{e}^{-\mathrm{s}z/\lambda_2(\mathrm{s})} & \\ & & \textit{etc.} \end{pmatrix}, \tag{11}$$

in which λ_i $(i=1,2,\cdots,14)$ are the eigenvalues of $\mathbf{A}^{*\text{-}1}\mathbf{B}$.

As the state vector at any position could be expressed, a solution of a pipe section could be obtained. For the single section of a straight or a curved pipe, boundaries are set at two ends of this section, where $z=0$ and $z=L$ of the domain $0\le z\le L$. Following the method described in Ref. [6], there will be seven relations at each end, namely

$$\mathbf{D_0}(\mathrm{s})\tilde{\boldsymbol{\phi}}(0,\mathrm{s})=\mathbf{Q_0}(\mathrm{s}),\ \mathbf{D_L}(\mathrm{s})\tilde{\boldsymbol{\phi}}(L,\mathrm{s})=\mathbf{Q_L}(\mathrm{s}) \tag{12}$$

where $\mathbf{D_0}$ and $\mathbf{D_L}$ are boundary matrices (7×14), and $\mathbf{Q_0}$ and $\mathbf{Q_L}$ are external excitation vectors (7×1) at two ends. Then a boundary equation could be derived from Eq. (9) and (12)

$$\tilde{\boldsymbol{\phi}}(0,\mathrm{s}) = \mathbf{D}^{*\text{-}1}(\mathrm{s})\mathbf{Q}(\mathrm{s}), \tag{13}$$

in which

$$\mathbf{D}^{*}(\mathrm{s}) = \begin{pmatrix} \mathbf{D_0}(\mathrm{s}) \\ \mathbf{D_L}(\mathrm{s})\mathbf{M}(L,\mathrm{s}) \end{pmatrix}, \text{ and } \mathbf{Q}(\mathrm{s}) = \begin{pmatrix} \mathbf{Q_0}(\mathrm{s}) \\ \mathbf{Q_L}(\mathrm{s}) \end{pmatrix}. \tag{14}$$

Hence, variables of $\tilde{\boldsymbol{\phi}}(z,\mathrm{s})$ at any position could be calculated by $\tilde{\boldsymbol{\phi}}(0,\mathrm{s})$ and $\mathbf{M}(z,\mathrm{s})$.

2.2. Boundary and excitation

The very crucial step for solving the FSI model using the aforementioned method is to obtain the boundary matrix and excitation matrix. In this area, Davidson *et al*. [15], Lesmez [22], Tentarelli [23], and Tijsseling [45] discussed kinds of boundary conditions, and Zhang *et al*. [6] gave both boundary matrices of the axial and lateral excitation. Although the basic idea of boundary and excitation are defined by the previous work, complex constraints involving extra mass, spring and damping have not yet been presented, and these will be studied in this subsection.

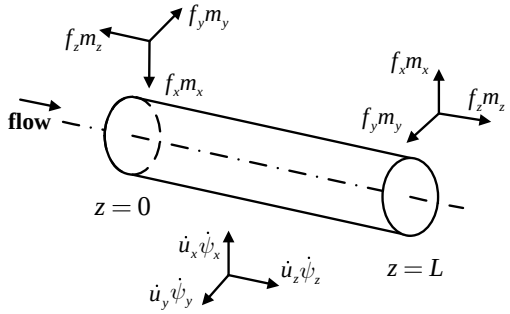

Fig.2 Coordinate system of a single pipe section.

As for the 14-equation model of a single pipe section, force equilibrium and motion direction are shown in Fig.2, defining tensile forces to be positive. Based on the theory of Bond Graphs [46], one can assume a virtual node existing between pipe end and external excitation, although sometimes this node may be a real part of pipe as it has mass. As this node of mechanical field is actually an effort junction (or 1-junction), efforts which are always forces or angular moments sum to zero, and flows which refer to linear or angular velocity are equal [46,47]. So one can obtain the force balance at the end of pipe as shown in Fig.3, providing one chooses this node as the object. F_x, F_y and F_z are constraint forces in three directions, and F_r is the external force in axial direction. Constraint moments (T_x, T_y and T_z) are shown as well. Additionally, the fluid force $A_f P$ shown in Fig.3 would not be considered in the case of an open end.

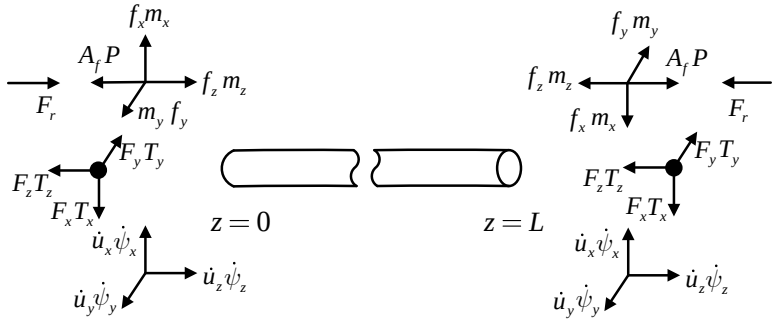

Fig.3 Coordinate systems of nodes at two pipe ends.

As boundary equations (Eq.(12)) are based on force equilibrium, excitation vectors at the two ends can be defined as

$$\mathbf{Q_0}(\mathrm{s}) = \begin{matrix} V_e(0,\mathrm{s}) & f_{ez}(0,\mathrm{s}) & f_{ey}(0,\mathrm{s}) & m_{ex}(0,\mathrm{s}) & f_{ex}(0,\mathrm{s}) & m_{ey}(0,\mathrm{s}) & m_{ez}(0,\mathrm{s}) \end{matrix}^{\mathrm{T}},$$

$$\mathbf{Q_L}(\mathrm{s}) = \begin{matrix} V_e(L,\mathrm{s}) & f_{ez}(L,\mathrm{s}) & f_{ey}(L,\mathrm{s}) & m_{ex}(L,\mathrm{s}) & f_{ex}(L,\mathrm{s}) & m_{ey}(L,\mathrm{s}) & m_{ez}(L,\mathrm{s}) \end{matrix}^{\mathrm{T}}, \quad (15)$$

indicating that there is one fluid equation describing liquid boundary and six force (or moment) balance equations relating to mechanical motions in three planes at each pipe end. And excitation of the fluid velocity is represented by the first element of the excitation vector. Then the boundary matrices of closed ends, considering arbitrary constraints of elasticity, damping and inertia, can be expressed as

$$\mathbf{D_0}(\mathrm{s}) = \begin{pmatrix} 1 & 0 & -1 & 0 & & & & & & & & & & \\ 0 & -A_f & -Z_{z(0)} & 1 & & & & & & & & & & \\ & & & & -Z_{y(0)} & 1 & 0 & 0 & & & & & & \\ & & & & 0 & 0 & -Y_{x(0)} & 1 & & & & & & \\ & & & & & & & & -Z_{x(0)} & 1 & 0 & 0 & & \\ & & & & & & & & 0 & 0 & -Y_{y(0)} & 1 & & \\ & & & & & & & & & & & & -Y_{z(0)} & 1 \end{pmatrix},$$

$$\mathbf{D_L}(\mathrm{s}) = \begin{pmatrix} 1 & 0 & -1 & 0 & & & & & & & & & & \\ 0 & -A_f & Z_{z(L)} & 1 & & & & & & & & & & \\ & & & & Z_{y(L)} & 1 & 0 & 0 & & & & & & \\ & & & & 0 & 0 & Y_{x(L)} & 1 & & & & & & \\ & & & & & & & & Z_{x(L)} & 1 & 0 & 0 & & \\ & & & & & & & & 0 & 0 & Y_{y(L)} & 1 & & \\ & & & & & & & & & & & & Y_{z(L)} & 1 \end{pmatrix}, \quad (16)$$

where linear impedances of constraint forces are listed as

$$Z_{x(i)} = \frac{k_{x(i)}}{\mathrm{s}} + \zeta_{x(i)} + m_{c(i)}\mathrm{s}, \quad Z_{y(i)} = \frac{k_{y(i)}}{\mathrm{s}} + \zeta_{y(i)} + m_{c(i)}\mathrm{s}, \quad Z_{z(i)} = \frac{k_{z(i)}}{\mathrm{s}} + \zeta_{z(i)} + m_{c(i)}\mathrm{s},$$

and angular impedances of moments are

$$Y_{x(i)}=\frac{t_{x(i)}}{\mathrm{s}}+\gamma_{x(i)}+I_{cx(i)}\mathrm{s},\ Y_{y(i)}=\frac{t_{y(i)}}{\mathrm{s}}+\gamma_{y(i)}+I_{cy(i)}\mathrm{s},\ Y_{z(i)}=\frac{t_{z(i)}}{\mathrm{s}}+\gamma_{z(i)}+I_{cz(i)}\mathrm{s},$$

$i=0$ or L. Herein k, t, ζ, γ, m_c, I_c are linear stiffness, torsional stiffness, linear damping, torsional damping, extra mass, and extra moment of inertia of supports respectively. Note that $\mathbf{D_0}(\mathrm{s})$ and $\mathbf{D_L}(\mathrm{s})$ are different, due to the difference of positive directions defined by the coordinate systems at the two ends.

Fluid boundary conditions could be reflected by the first element of the excitation vector. If the fluid velocity is considered, the boundary equation can be written as

$$V-\dot{u}_z=V_e. \tag{17}$$

For a closed end, V_e equals zero. If the excitation is a sudden valve closure, which may be treated as a step change of the fluid velocity, for example -1 m s^{-1}, then V_e would be $-1/\mathrm{s}$. Another common case is the open pipe end (assuming $z=L$), which means liquid excitation is zero. Then the boundary matrix would be

$$\mathbf{D_L}(\mathrm{s})=\begin{pmatrix}
0 & 1 & 0 & 0 & & & & & & & & \\
0 & 0 & Z_{z(L)} & 1 & & & & & & & & \\
 & & & & Z_{y(L)} & 1 & 0 & 0 & & & & \\
 & & & & 0 & 0 & Y_{x(L)} & 1 & & & & \\
 & & & & & & & & Z_{x(L)} & 1 & 0 & 0 \\
 & & & & & & & & 0 & 0 & Y_{y(L)} & 1 \\
 & & & & & & & & & & & \\
 & & & & & & & & & & Y_{z(L)} & 1
\end{pmatrix}, \tag{18}$$

while

$$\mathbf{Q_L}(\mathrm{s})=\begin{matrix}P_e(L,\mathrm{s}) & f_{ez}(L,\mathrm{s}) & f_{ey}(L,\mathrm{s}) & m_{ex}(L,\mathrm{s}) & f_{ex}(L,\mathrm{s}) & m_{ey}(L,\mathrm{s}) & m_{ez}(L,\mathrm{s})\end{matrix}^{\mathrm{T}}, \tag{19}$$

and P_e equals zero for opening to the air. Note that the first element in excitation vector changes from fluid velocity to fluid pressure. So there exists a flexibility of choosing fluid excitation, due to different fluid boundary conditions.

The behaviour of a hydraulic piping system is significantly influenced by various valves, clamps, and support conditions. In the present method, valves, clamps and masses attached to the pipeline are basically treated as lumped components, described by extra stiffness, inertia and damping coefficients. In the case of free or rigid supports, the system can be calculated by setting the stiffness as zero or a large number respectively. The hydraulic pipe clamps could be treated as lumped constraints with mass, structural stiffness, and viscoelastic damping effect.

2.3. Middle constraint

The cascaded pipeline (Fig.4) is the most common configuration in actual pipe systems, which might consist of straight and curved sections. Lesmez [22] investigated extra mass and spring force in the middle of a straight pipe. Budny and Wiggert *et al*. [48] studied the influence of the structural damping imposed on pipes. The clamp stiffness was included in the 14-equation

model of a long pipe by Kwong and Edge [28]. Heinsbroek and Tijsseling [49] studied a large-scale pipe system which was supported by linear springs. Tijsseling and Vardy [50] researched a water-filled pipe resting on a supporting cylinder, where the pipe-rack interface can be modelled by the friction force. Wu and Shih [51] analysed dynamics of multi-span pipe with extra load in the middle of pipeline. Yang *et al*. [52] studied the multi-span pipeline with rigid supports. Liu and Li [30] proposed point transfer matrices considering elastic constraints for the 14-equation model of FSI. This subsection is focused on a uniform expression of middle constraints, including extra stiffness, damping, and inertia.

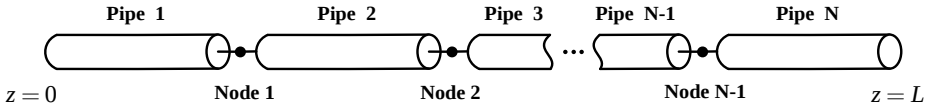

Fig.4 The sections and nodes of a pipeline.

A constraint node is introduced to describe the relation where a complex constraint or a sudden change in geometry exists, which is the same as nodes at pipe ends mentioned in the last subsection. Concentrating on this node, force and moment equilibrium as well as motion direction could be obtained, shown in Fig.5.

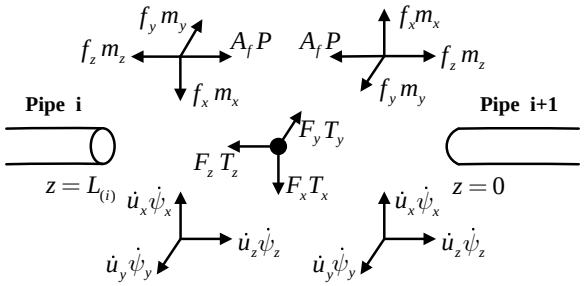

Fig.5 Coordinate system of the i node at the position of middle constraint.

Based on the definition of point transfer matrix given by TMM, the relation between state vectors at two sides of the constraint node could be expressed as

$$\tilde{\boldsymbol{\phi}}_{i+1}(0,\mathrm{s}) = \mathbf{N}_i(\mathrm{s})\tilde{\boldsymbol{\phi}}_i(L_i,\mathrm{s})\,. \tag{20}$$

The constraint matrix here is

$$\mathbf{N}_i(\mathrm{s})=\begin{pmatrix}
\frac{A_{f(i)}}{A_{f(i+1)}} & & & 1-\frac{A_{f(i)}}{A_{f(i+1)}} & & & & & & & & & & \\
& 1 & & & & & & & & & & & & \\
& & 1 & & & & & & & & & & & \\
& A_{f(i+1)}-A_{f(i)} & Z_{z(i)} & 1 & & & & & & & & & & \\
& & & & 1 & & & & & & & & & \\
& & & & Z_{y(i)} & 1 & & & & & & & & \\
& & & & & & 1 & & & & & & & \\
& & & & & & Y_{x(i)} & 1 & & & & & & \\
& & & & & & & & 1 & & & & & \\
& & & & & & & & Z_{x(i)} & 1 & & & & \\
& & & & & & & & & & 1 & & & \\
& & & & & & & & & & Y_{y(i)} & 1 & & \\
& & & & & & & & & & & & 1 & \\
& & & & & & & & & & & & Y_{z(i)} & 1
\end{pmatrix}, \quad (21)$$

where linear impedances ($Z_{x(i)}, Z_{y(i)}, Z_{z(i)}$), and angular impedances ($Y_{x(i)}, Y_{y(i)}, Y_{z(i)}$) of constraints are defined in Eq.(16), while i denotes the number of middle constraint (or constraint node). The matrix is similar to the boundary matrix but larger (14×14). Note that the constraint matrix revealed here is a point matrix from the concept of TMM, indicating a discontinuity between two pipe sections, and might equal the identity matrix when no constraint exists and areas of adjacent sections are equal. In the same way as the boundary matrix, the constraint matrix can model free and rigid supports, as well as clamps which may have complex impedance in practice.

To solve the cascaded pipeline, an overall transfer matrix (or global transfer matrix [21]) relating state vectors at two ends of the pipeline can be expressed by a systematic multiplication of the field and the point transfer matrices.

$$\mathbf{M}_{\mathbf{global}}(\mathrm{s})=\mathbf{M}_N(L_N,\mathrm{s})\mathbf{N}_{N-1}(\mathrm{s})\cdots\mathbf{N}_i(\mathrm{s})\mathbf{M}_i(L_i,\mathrm{s})\cdots\mathbf{N}_1(\mathrm{s})\mathbf{M}_1(L_1,\mathrm{s}),1\le i\le N-1 \quad (22)$$

in which $\mathbf{M}_i$ is the field matrix of a pipe section, $\mathbf{N}_i$ is the point matrix of a middle constraint, and L_i is the length of a section. Hence, the cascaded piping system could be solved by aforementioned method, and the state vector at one end would be

$$\tilde{\boldsymbol{\phi}}_1(0,\mathrm{s})=\mathbf{D}^{*\text{-}1}(\mathrm{s})\mathbf{Q}(\mathrm{s}), \quad (23)$$

where

$$\mathbf{D}^{*}(\mathrm{s})=\begin{pmatrix}\mathbf{D_0}(\mathrm{s})\\ \mathbf{D_L}(\mathrm{s})\mathbf{M_{global}}(\mathrm{s})\end{pmatrix}, \quad \mathbf{Q}(\mathrm{s})=\begin{pmatrix}\mathbf{Q_0}(\mathrm{s})\\ \mathbf{Q_L}(\mathrm{s})\end{pmatrix}. \quad (24)$$

Then variables of $\tilde{\boldsymbol{\phi}}(z,\mathrm{s})$ at any position could be expressed.

In this subsection, middle constraints or complex supports in the pipeline are modelled as point transfer matrices, and included in the overall transfer matrix of the system. Using the general solution of a two-port pipe system mentioned in section 2.1, the cascaded pipe system

with diverse constraints could be solved.

3. Solution of branched pipeline

Apart from the cascaded configuration, T-junctions are widely used in actual pipelines to form branched systems. In this section, the modelling and solution of T-junctions with 14 variables are introduced in 3.1, using the expression of point transfer matrix. A novel point is that constraints at the position of T-junction will be included. Based on the modelling of T-junction, a two-branch pipeline can be modelled and solved (Appendix C). Furthermore, a general solution method of multi-branch pipes is proposed in 3.2. A rotation matrix to describe the complex spatial structure is discussed as well.

3.1. Solution of T-junction considering constraints

The literature shows that many experiments have been performed in systems with elbows or curved pipes, but just a few in systems with branches. Tentarelli [23] studied a three-port junction and gave the equation representing three relations in matrix form. Vardy *et al*. [53] reported an experiment of T-piece pipe which can move freely in a nearly horizontal plane, where FSI effect was validated precisely. Experiments on this apparatus were continued by Tijsseling *et al*. [54,55], and the 14-order point transfer matrix of T-junction was developed [56]. The method presented here follows the previous research, modelling the T-junction as a point transfer matrix rather than a field transfer matrix, and a solution for the three-port pipe is developed from the method mentioned in section 2. Fourteen equations for T-junction just considering kinematic movements of fluid and solid are presented in Appendix B, and coordinate systems and force balances at T-junction node are depicted in Fig.6.

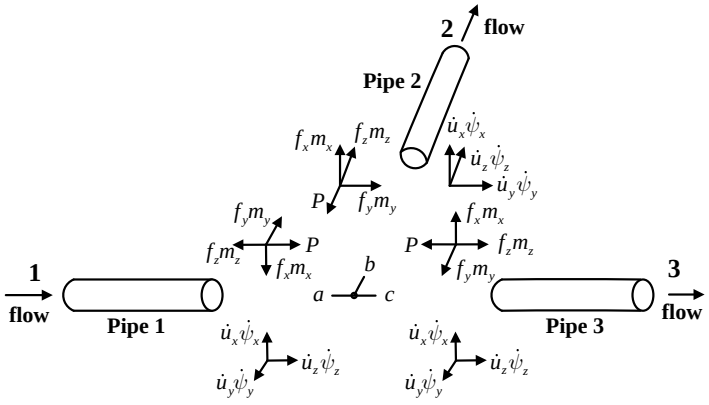

Fig.6 Coordinate systems of T-junction node connecting three straight sections.

The state vector at any port of T-junction node could be expressed by those of the other two ports. For the purpose of a general approach of multi-branch pipeline, local coordinate systems are defined as Fig.6, and the transfer relation can be expressed in matrix form

$$\begin{pmatrix} \tilde{\boldsymbol{\phi}}_3(0,\mathrm{s}) \\ \mathbf{0} \end{pmatrix} = \mathbf{T}(s) \begin{pmatrix} \tilde{\boldsymbol{\phi}}_1(L_1,\mathrm{s}) \\ \tilde{\boldsymbol{\phi}}_2(0,\mathrm{s}) \end{pmatrix}. \tag{25}$$

Here $\mathbf{T}$ is the point transfer matrix (21×28) of T-junction node, L_i is the length of pipe i (i =1,2,3), and $\tilde{\boldsymbol{\phi}}_1(L_1,\mathrm{s})$, $\tilde{\boldsymbol{\phi}}_2(0,\mathrm{s})$ and $\tilde{\boldsymbol{\phi}}_3(0,\mathrm{s})$ are Laplace-transformed state vectors at three ports of this junction node (Fig.6). One can also obtain the expression with state vectors at three pipe ends,

$$\begin{pmatrix} \mathbf{M}_3^{-1}(L_3,\mathrm{s})\tilde{\boldsymbol{\phi}}_3(L_3,\mathrm{s}) \\ \mathbf{0} \end{pmatrix} = \mathbf{T}(s) \begin{pmatrix} \mathbf{M}_1(L_1,\mathrm{s})\tilde{\boldsymbol{\phi}}_1(0,\mathrm{s}) \\ \mathbf{M}_2^{-1}(L_2,\mathrm{s})\tilde{\boldsymbol{\phi}}_2(L_2,\mathrm{s}) \end{pmatrix}, \tag{26}$$

in which, $\mathbf{M}_1$, $\mathbf{M}_2$ and $\mathbf{M}_3$ are field transfer matrices of three pipe sections connecting to the T-junction. $\tilde{\boldsymbol{\phi}}_1(0,\mathrm{s})$, $\tilde{\boldsymbol{\phi}}_2(L_2,\mathrm{s})$ and $\tilde{\boldsymbol{\phi}}_3(L_3,\mathrm{s})$ is state vector at each pipe end respectively.

To solve this T-shaped pipe, one can obtain its boundary equation as

$$\begin{pmatrix} \mathbf{D}_1(\mathrm{s})\tilde{\boldsymbol{\phi}}_1(0,\mathrm{s}) \\ \mathbf{D}_2(\mathrm{s})\tilde{\boldsymbol{\phi}}_2(L_2,\mathrm{s}) \\ \mathbf{D}_3(\mathrm{s})\tilde{\boldsymbol{\phi}}_3(L_3,\mathrm{s}) \end{pmatrix} = \begin{pmatrix} \mathbf{Q}_1(\mathrm{s}) \\ \mathbf{Q}_2(\mathrm{s}) \\ \mathbf{Q}_3(\mathrm{s}) \end{pmatrix}. \tag{27}$$

Based on Eq.(26), the boundary equation at the third pipe end can be derived as

$$\begin{pmatrix} \mathbf{Q}_3(\mathrm{s}) \\ \mathbf{0} \end{pmatrix}_{14\times 1} = \mathbf{H}(\mathrm{s})\mathbf{G}(\mathrm{s})\mathbf{T}(\mathrm{s})\mathbf{M}_{\mathbf{T}}(\mathrm{s}) \begin{pmatrix} \tilde{\boldsymbol{\phi}}_1(0,\mathrm{s}) \\ \tilde{\boldsymbol{\phi}}_2(L_2,\mathrm{s}) \end{pmatrix}, \tag{28}$$

where

$$\mathbf{H}(\mathrm{s}) = \begin{pmatrix} \mathbf{D}_3(\mathrm{s}) & \mathbf{0} \\ \mathbf{0} & \mathbf{I}_{7\times 7} \end{pmatrix}_{14\times 21}, \tag{29}$$

$$\mathbf{G}(\mathrm{s}) = \begin{pmatrix} \mathbf{M}_3(L_3,\mathrm{s}) & \mathbf{0} \\ \mathbf{0} & \mathbf{I}_{7\times 7} \end{pmatrix}_{21\times 21}, \tag{30}$$

and

$$\mathbf{M}_{\mathbf{T}}(\mathrm{s}) = \begin{pmatrix} \mathbf{M}_1(L_1,\mathrm{s}) & \mathbf{0} \\ \mathbf{0} & \mathbf{M}_2^{-1}(L_2,\mathrm{s}) \end{pmatrix}_{28\times 28}. \tag{31}$$

Hence, the solution of a T-shaped pipe could be expressed as

$$\begin{pmatrix} \mathbf{D}_1(\mathrm{s}) & \mathbf{0} \\ \mathbf{0} & \mathbf{D}_2(\mathrm{s}) \\ \mathbf{H}(\mathrm{s})\mathbf{G}(\mathrm{s})\mathbf{T}(\mathrm{s})\mathbf{M}_{\mathbf{T}}(\mathrm{s}) \end{pmatrix}_{28\times 28} \begin{pmatrix} \tilde{\boldsymbol{\phi}}_1(0,\mathrm{s}) \\ \tilde{\boldsymbol{\phi}}_2(L_2,\mathrm{s}) \end{pmatrix}_{28\times 1} = \begin{pmatrix} \mathbf{Q}_1(\mathrm{s}) \\ \mathbf{Q}_2(\mathrm{s}) \\ \mathbf{Q}_3(\mathrm{s}) \\ \mathbf{0} \end{pmatrix}_{28\times 1}. \tag{32}$$

Once $\tilde{\boldsymbol{\phi}}_1(0,\mathrm{s})$ and $\tilde{\boldsymbol{\phi}}_2(L_2,\mathrm{s})$ are obtained, the third state vector $\tilde{\boldsymbol{\phi}}_3(L_3,\mathrm{s})$ can be calculated by

$$\tilde{\boldsymbol{\phi}}_3(L_3,\mathrm{s}) = \begin{matrix}\mathbf{I}_{14\times14} & \mathbf{0}_{14\times21}\end{matrix}\mathbf{G}(\mathrm{s})\mathbf{T}(\mathrm{s})\mathbf{M}_{\mathbf{T}}(\mathrm{s})\begin{pmatrix}\tilde{\boldsymbol{\phi}}_1(0,\mathrm{s})\\ \tilde{\boldsymbol{\phi}}_2(L_2,\mathrm{s})\end{pmatrix}. \tag{33}$$

Hence, variables at any position could be obtained.

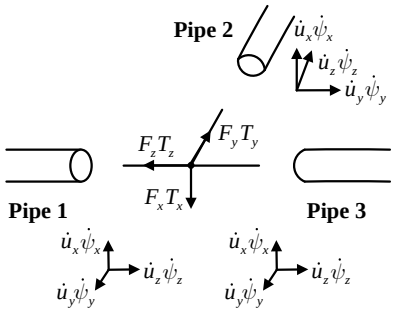

Fig.7 Constraint at position of T-junction.

A constraint or additional mechanical impedance existing at the position of a T-junction node, such as the extra mass of a T-piece fitting, could be expressed as the constraint matrix $\mathbf{N}$ (Eq.(21)). Assuming directions of constraint forces and moments are defined as Fig.7, the constraint matrix can be contained in the relation as

$$\begin{pmatrix}\mathbf{M}_3^{-1}(L_3,\mathrm{s})\tilde{\boldsymbol{\phi}}_3(L_3,\mathrm{s})\\ \mathbf{0}\end{pmatrix} = \mathbf{T}(\mathrm{s})\begin{pmatrix}\mathbf{N}(\mathrm{s})\mathbf{M}_1(L_1,\mathrm{s})\tilde{\boldsymbol{\phi}}_1(0,\mathrm{s})\\ \mathbf{M}_2^{-1}(L_2,\mathrm{s})\tilde{\boldsymbol{\phi}}_2(L_2,\mathrm{s})\end{pmatrix}, \tag{34}$$

which means that the constraint matrix can be simply cascaded in the transfer matrix of pipe 1. It should be pointed out that $\mathbf{N}$ could be contained in any transfer matrix of three connecting pipes relating to different definitions of constraint's direction. So one can obtain the method considering constraints by modifying the transfer matrix of any connecting section, which means to replace $\mathbf{M}_1$, $\mathbf{M}_2$ or $\mathbf{M}_3$ with $\mathbf{NM}_1$, $\mathbf{M}_2\mathbf{N}$ or $\mathbf{M}_3\mathbf{N}$ respectively.

3.2. General solution of multi-branch pipeline

Pipelines with more than one branch are common in hydraulic systems, which may consist of several bypass circuits and different fluid or mechanical excitation. The multi-branch pipe system could seem as a series of cascaded T-piece pipes (Fig.8), and a general solution is proposed in this subsection.

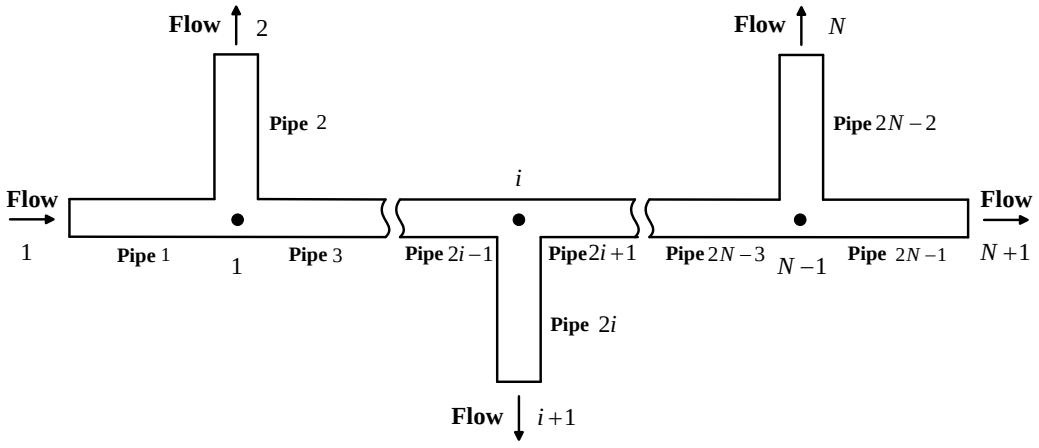

Fig.8 Schematic diagram of multi-branch pipe system.

The multi-branch pipeline shown in Fig.8 has $N-1$ T-junctions, $N+1$ ports and $2N-1$ pipe sections. Its solution method can be extended from derivation of two-branch system presented in Appendix C, written as

$$\begin{pmatrix} \mathbf{D}_1(\mathrm{s}) & & & \\ & \mathbf{D}_2(\mathrm{s}) & & \\ & & \ddots & \\ & & & \mathbf{D}_N(\mathrm{s}) \\ \mathbf{H}(\mathrm{s})\mathbf{F}_{N\text{-}1}(\mathrm{s})\cdots\mathbf{F}_1(\mathrm{s})\mathbf{L}\mathbf{M}_{\mathbf{T}}(\mathrm{s}) & & & \end{pmatrix}_{14N\times 14N} \begin{pmatrix} \tilde{\boldsymbol{\phi}}_1(0,\mathrm{s}) \\ \vdots \\ \tilde{\boldsymbol{\phi}}_{2i}(L_{2i},\mathrm{s}) \\ \vdots \\ \tilde{\boldsymbol{\phi}}_{2N-2}(L_{2N-2},\mathrm{s}) \end{pmatrix}_{14N\times 1} = \begin{pmatrix} \mathbf{Q}_1(\mathrm{s}) \\ \mathbf{Q}_2(\mathrm{s}) \\ \vdots \\ \mathbf{Q}_{N+1}(\mathrm{s}) \\ \mathbf{0} \end{pmatrix}_{14N\times 1}, \quad (35)$$

where

$$\mathbf{H}(\mathrm{s}) = \begin{pmatrix} \mathbf{D}_{N+1}(\mathrm{s}) & \mathbf{0} \\ \mathbf{0} & \mathbf{I}_{(7N-7)\times(7N-7)} \end{pmatrix}_{7N\times(7N+7)},$$

$$\mathbf{F}_i(\mathrm{s}) = \begin{pmatrix} \mathbf{I}_{(14N-14-14i)\times(14N-14-14i)} & & \\ & \mathbf{G}_i(\mathrm{s})\mathbf{T}_i(\mathrm{s})\mathbf{J} & \\ & & \mathbf{I}_{(7i-7)\times(7i-7)} \end{pmatrix}_{(14N-7i)\times(14N-7i+7)},$$

$$\mathbf{G}_i(\mathrm{s}) = \begin{pmatrix} \mathbf{M}_{2i+1}(L_{2i+1},\mathrm{s}) & \mathbf{0} \\ \mathbf{0} & \mathbf{I}_{7\times 7} \end{pmatrix}_{21\times 21},$$

$$\mathbf{J} = \begin{pmatrix} \mathbf{0} & \mathbf{I}_{14\times 14} \\ \mathbf{I}_{14\times 14} & \mathbf{0} \end{pmatrix},$$

$$\mathbf{L} = \begin{pmatrix} & & \mathbf{I}_{14\times 14} \\ & \iddots & \\ \mathbf{I}_{14\times 14} & & \end{pmatrix}_{14N\times 14N},$$

$$\mathbf{M}_{\mathbf{T}}(\mathrm{s})=\begin{pmatrix}\mathbf{M}_1(L_1,\mathrm{s}) & & & & \\ & \ddots & & & \\ & & \mathbf{M}_{2i}^{-1}(L_{2i},\mathrm{s}) & & \\ & & & \ddots & \\ & & & & \mathbf{M}_{2N-2}^{-1}(L_{2N-2},\mathrm{s})\end{pmatrix}_{14N\times 14N},$$

$$i=1,\cdots,N-1,\quad N\geq 2,$$

and $\mathbf{T}_i(\mathrm{s})$ is the point transfer matrix at the i T-junction node, while $\mathbf{M}_j(L_j,\mathrm{s})$ is the global transfer matrix of pipe j ($j=1,\cdots,2N-1,\quad N\geq 2$), which might be multiplied by the constraint matrix $\mathbf{N}(\mathrm{s})$ when constraints at position of T-junction are considered. Then the state vector at port $N+1$ can be calculated by

$$\tilde{\boldsymbol{\phi}}_{2N-1}(L_{2N-1},\mathrm{s})=\begin{matrix}\mathbf{I}_{14\times 14} & \mathbf{0}_{14\times(7N+7)}\end{matrix}\mathbf{F}_{N\text{-}1}(\mathrm{s})\cdots\mathbf{F}_1(\mathrm{s})\mathbf{L}\mathbf{M}_{\mathbf{T}}(\mathrm{s})\begin{pmatrix}\tilde{\boldsymbol{\phi}}_1(0,\mathrm{s})\\ \vdots\\ \tilde{\boldsymbol{\phi}}_{2i}(L_{2i},\mathrm{s})\\ \vdots\\ \tilde{\boldsymbol{\phi}}_{2N-2}(L_{2N-2},\mathrm{s})\end{pmatrix}_{14N\times 1}. \quad (36)$$

One may find that intermediate matrices in this general solution are nearly diagonal ($\mathbf{H}$, $\mathbf{F}$, $\mathbf{G}$, $\mathbf{M}_{\mathbf{T}}$) or anti-diagonal ($\mathbf{J}$, $\mathbf{L}$), which may reduce the complication of numerical calculation due to properties of sparse matrices, although the solution matrix will become larger as the number of branches increases.

To solve a piping system with 3-dimensional configuration rather than in-plane structure, the definition of the local coordinate system on each pipe section is significant. The basic idea to model this spatial system is introducing a rotation matrix to describe the relation between two adjacent coordinate systems (Fig.9). The rotation matrix was utilised by Davidson *et al*. [18], Tentarelli [23], and Jiao *et al*. [29], and was defined as a point transfer matrix which only relates to the angle between two coordinate systems, expressed as

$$\tilde{\boldsymbol{\phi}}_{i+1}(0,\mathrm{s})=\mathbf{R}_i(\varphi)\tilde{\boldsymbol{\phi}}_i(L_i,\mathrm{s}). \quad (37)$$

where

$$\mathbf{R}_i(\varphi)=\begin{pmatrix}
1 & & & & & & & & & & & \\
& 1 & & & & & & & & & & \\
& & 1 & & & & & & & & & \\
& & & 1 & & & & & & & & \\
& & & & \cos\varphi & & & & -\sin\varphi & & & \\
& & & & & \cos\varphi & & & & -\sin\varphi & & \\
& & & & & & \cos\varphi & & & & \sin\varphi & \\
& & & & & & & \cos\varphi & & & & \sin\varphi \\
& & & & \sin\varphi & & & & \cos\varphi & & & \\
& & & & & \sin\varphi & & & & \cos\varphi & & \\
& & & & & & -\sin\varphi & & & & \cos\varphi & \\
& & & & & & & -\sin\varphi & & & & \cos\varphi \\
& & & & & & & & & & 1 & \\
& & & & & & & & & & & 1
\end{pmatrix}, \quad (38)$$

and φ is the angle between two adjacent coordinate systems, defining anticlockwise rotation as the positive direction when z axis points towards the observer. Moreover, the rotation matrix $\mathbf{R}$ can be treated as a kind of constraint matrix in practice. So the relation of two state vectors at the ends of the pipe series shown in Fig.9 would be

$$\tilde{\boldsymbol{\phi}}_{i+1}(L_{i+1},\mathrm{s})=\mathbf{M}_{i+1}(L_{i+1},\mathrm{s})\mathbf{R}_i(\varphi)\mathbf{N}_i(\mathrm{s})\mathbf{M}_i(L_i,\mathrm{s})\tilde{\boldsymbol{\phi}}_i(0,\mathrm{s}), \quad (39)$$

in which $\mathbf{M}_i$ is the field transfer matrix of pipe i, and $\mathbf{N}_i$ is the middle constraint matrix. Note that the x axis of a curved section (Fig.9) and T-junction (Fig.6) are always perpendicular to the plane determined by coordinate systems, so rotation matrices are commonly used in the modelling of pipelines with bends and branches.

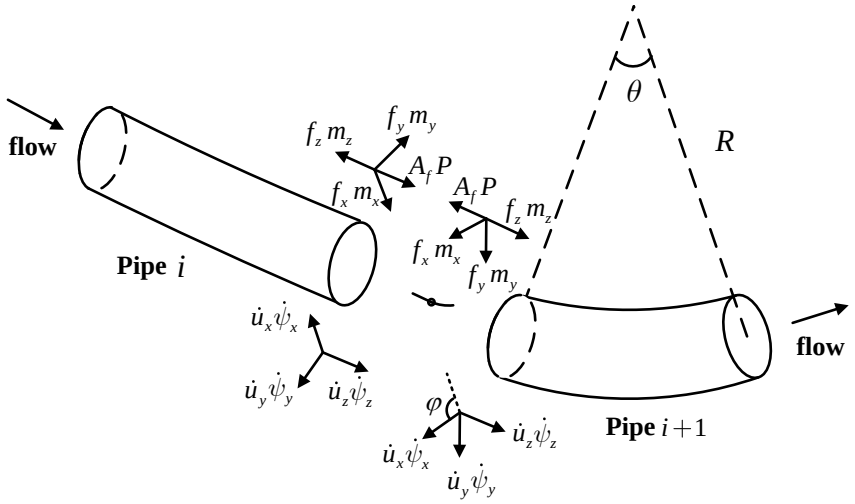

Fig.9 Coordinate system of the i node at position of local coordinate system's change.

4. Experiments

In this section, experimental measurements are presented and compared with predicted

results. One experiment is a single T-shaped pipe which has been investigated previously [53,54], and the other is a two-branch pipe which has not been carried out hitherto. All pipe sections were closed at their ends and filled with oil, and hung by soft strings (string length 0.6 m) which allowed free motion in a nearly horizontal plane without significant restraints. The system was excited by the external impact of a steel rod also hung by strings, and the maximum displacement of pipe ends during vibrations in experiments here was estimated to be 4 cm. The design of the apparatus follows experiments reported in University of Dundee [53,54], which brings the important advantages of (i) no unknown support conditions, (ii) clearly defined excitation.

The first experiment is a T-shaped pipe system, chosen to demonstrate the FSI method considering constraints of extra mass, and test the effectiveness and accuracy of this system. The second experiment is a two-branch pipe which is designed to demonstrate the general solution of multi-branch pipe system. Tungum tubes, steel fittings and hydraulic oil, which are commonly used in hydraulic systems, are used in the experimental system, with material and geometrical properties listed in Table 1. The impact rod is made of steel, and its length and diameter are 218 mm and 38.2 mm respectively. The shape of rod's front is flat, and it is found to be difficult to achieve a perfect plane contact. This has a significant influence on the consistency and alignment of the force impact. This problem is discussed in section 4.1 for the T-shaped pipe.

The impact rod was hung by two strings which were attached on a movable rack. Before each kind of test, the lengths of two strings for the rod and the position of the rack were adjusted to ensure correct alignment of the steel rod and pipe system. To ensure that the rod moved along or perpendicularly to the central line of the pipe, a digital camera was mounted above the rod to record the motion of the rod when it was swinging. As the alignment was carried out visually, small errors were inevitable and caused some variation in the results.

Table 1 Material and geometrical properties of experimental system.

Pipe (Tungum)	*Fitting (Steel)*	*Oil*
Density 8520 kg m^{-3}	Density 7850 kg m^{-3}	Density 876 kg m^{-3}
Young's modulus 116.5 GPa	Young's modulus 207 GPa	Bulk modulus 1.5 GPa
Shear modulus 43.8 GPa	Shear modulus 79.6 GPa	Initial pressure
Poisson's ratio 0.33	Poisson's ratio 0.3	T-shaped pipe: 9.4 bar
Outer diameter 25.4 mm		Two-branch pipe: 10 bar
Pipe wall thickness 2.2 mm		

4.1. T-shaped pipe

To demonstrate the solution method of constraints and the accuracy of the measurement system, a T-shaped pipe system is constructed. A similar experiment has been carried out by Vardy and Tijsseling *et al*. [53,54], and the mass and dimensions of the T-junction were neglected in their simulation [56]. As the lengths of pipes in the apparatus built here are much

smaller, the effect of the fittings cannot be neglected. Only axial impacts were studied in the work at Dundee; in the current work lateral impacts are also studied.

The T-shaped pipe shown in Fig.10 consists of three straight pipes connected by one T-piece fitting, and all pipe ends are sealed by screwed taps. The impact rod was hung by strings, which may impose an axial or lateral impact on the pipe end. A small valve (0.2 kg) in the T-piece raised the static pressure in the system by means of a hydraulic pump. The oil was allowed to settle for more than 24 hours to eliminate air bubbles, and the fluid pressure was raised repeatedly until it stayed stable. The mean pressure was chosen to be much higher than saturation pressure to avoid air release and cavitation.

The T-piece fitting used in the experiment is a typical hydraulic junction with compression type couplings ("Bite-Lock" structure) at three ports. In the previous research [53-56], the T-piece fitting was considered as a lumped mass neglecting its dimensions. While experimental pipe systems constructed in this work are relatively smaller, the effect of connecting parts (couplings) and geometrical size changing moment arms can not be neglected. The three couplings of the T-piece were treated as thicker steel pipe sections (length: 28 mm). Although the cubic block ($40\times40\times40$ mm) in the middle of T-junction can be considered as a rigid part due to its high stiffness, the effect of the moment arms caused by dimensions cannot be neglected. Hence the block was modelled as a lumped mass plus three thick pipe sections (length 12 mm). Material properties of these thick sections were set to be the same as those of three couplings, and were modelled together with couplings. The lumped mass mentioned here was included in the constraint matrix for the T-junction. Tapped fittings made of steel were screwed into the pipe at three pipe ends, which were modelled as short pipe sections with inner radii equalling zero. The node diagram in Fig.10 was used, with the dimensions in Table 2. The total mass of the T-piece fitting plus the valve was 1.56 kg, so the lumped mass at node 4 would be 0.32 kg as the weight of three thick pipe sections was excluded. The pressure transducer mass (0.01kg) was neglected.

The pipe system was instrumented with pressure transducers and the accelerometer. Piezoelectric pressure transducers (MEAS EPX-N03-15B), as indicated by 'pt' in Fig.10, were positioned at the centre of end taps, recording the transient dynamic pressure. The piezoelectric accelerometer (Brüel & Kjær 4339) where 'ac' is indicated was also employed to measure the vibration along the axial direction. The pressure transducers and the accelerometer had natural frequencies of 120 kHz and 75 kHz respectively.

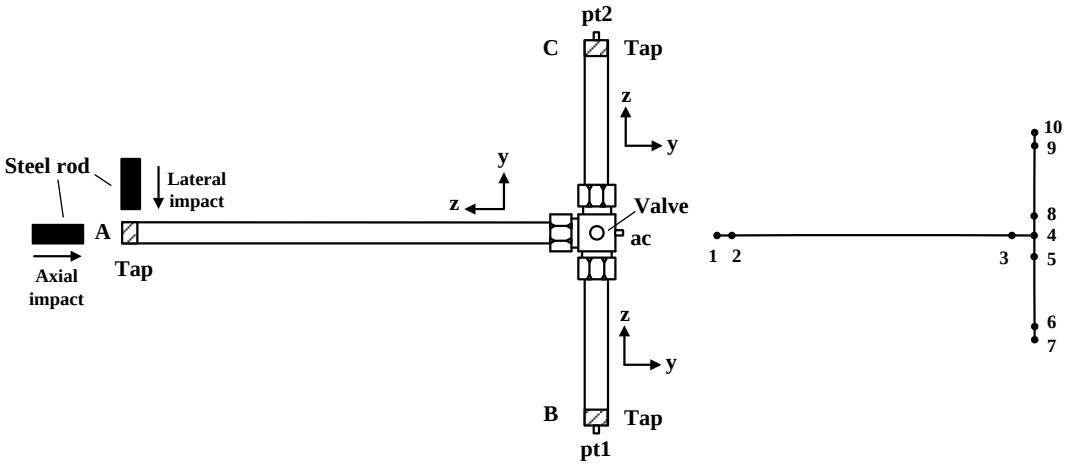

Fig.10 Schematic drawing of T-shaped pipe system.
(pt = pressure transducer, ac = accelerometer, Tap = tapped fitting)

Table 2 Dimensions of T-shaped pipe.

Position	*Length(mm)*	*Inner/outer radius(mm)*	*Material*
1-2, 6-7, 9-10	10	0.0 / 12.7	Steel
3-4, 4-5, 4-8	40	10.5 / 23.0	Steel
2-3	1160	10.5 / 12.7	Tungum
5-6, 8-9	524	10.5 / 12.7	Tungum

The impact rod offered a nearly axial force by hitting pipe end A axially, causing structural waves to propagate along the pipe. In the calculation, this force is approximated as an assumed constant axial force $F_{rod} \approx 600$ N persisting for a duration $T \approx 0.6$ ms. This can be expressed as $F_{rod}[1(t)-1(t-T)]$, and the Laplace transformed applied load is $(F_{rod}/\mathrm{s})(1-\mathrm{e}^{-sT})$ [6]. So the excitation vector at pipe end A could be written as

$$\mathbf{Q_A}(\mathrm{s}) = \begin{bmatrix} 0 & (F_{rod}/\mathrm{s})(1-\mathrm{e}^{-sT}) & 0 & 0 & 0 & 0 & 0 \end{bmatrix}^{\mathrm{T}}. \qquad (40)$$

Excitation vectors at the other two ends were null for no mechanical or fluid excitation at those positions. Using coordinate systems shown in Fig.6, one can define that the boundary matrix at position B is exactly $\mathbf{D_0}$ in Eq.(16), and those at position A and C equal $\mathbf{D_L}$. Hence, this system could be solved utilising the solution method for a T-shaped pipe in section 3.1. The frequency of simulation is $f = \mathrm{s}/(2\pi\mathrm{j})$, and the frequency resolution Δf is 0.5 Hz.

The acceleration and pressure were recorded in the time domain, and then transferred into frequency response using FFT. Some examples of time domain measurements are shown in figure 11. These show the early part of the transient; the full measurement is 1 s duration.

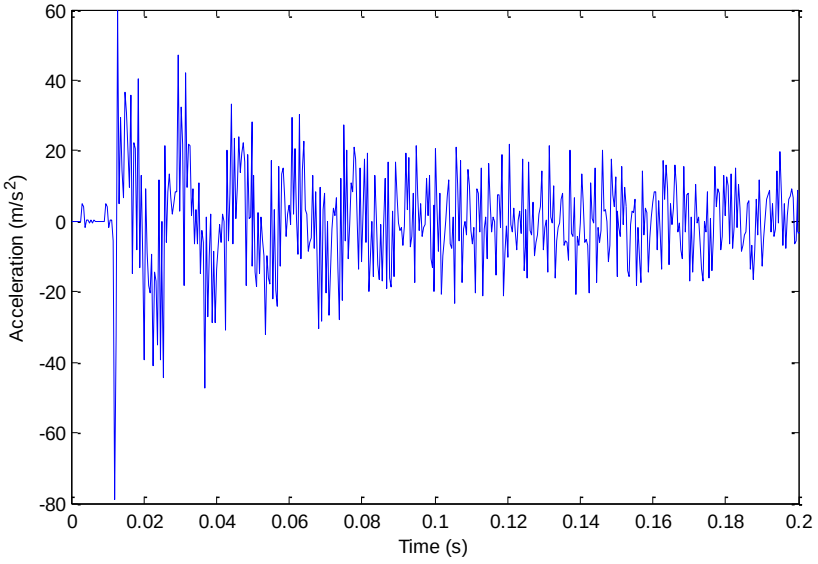

(a)

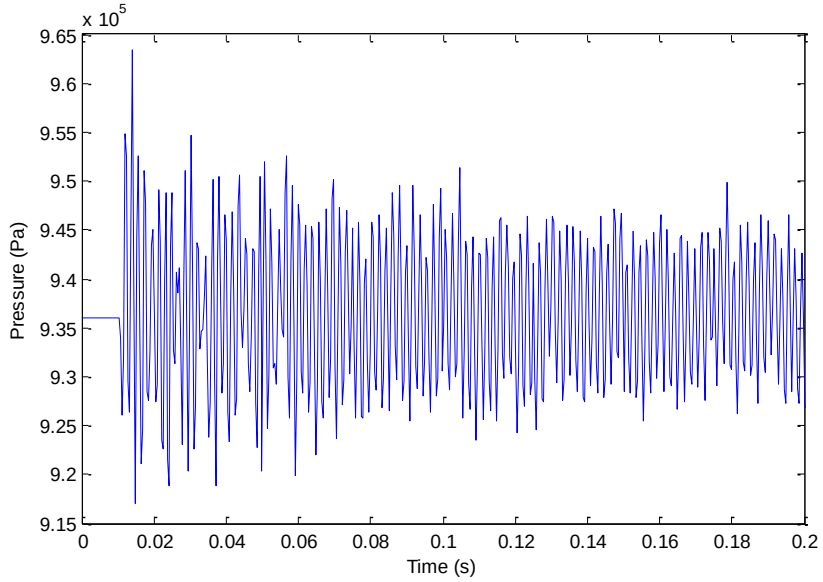

(b)

Fig.11 Examples of the time domain measurements.
(a) Axial acceleration of empty T-shaped pipe (axial impact);
(b) Fluid pressure in oil-filled T-shaped pipe (lateral impact).

Firstly, the empty T-shaped pipe excited by axial force was investigated. The fluid inside the pipe was air, so the density was 1.293 kg m^{-3} and the bulk modulus was 1.49×10^5 Pa. In Fig.12, the amplitude spectrum of measured axial acceleration is compared with numerical simulation results. The shape of the spectra differs because the spectrum of the actual excitation force is estimated and because of noise, but the frequency of the peaks can be compared as these indicate the natural frequencies of the system. The results show a good agreement in the frequencies of the peaks (62, 358, 911 and 1044 Hz of the simulation, compared with 60, 352, 900 and 1059 Hz of the measurement). The effectiveness and accuracy of this testing system is evident, and the modelling method considering constraints is validated.

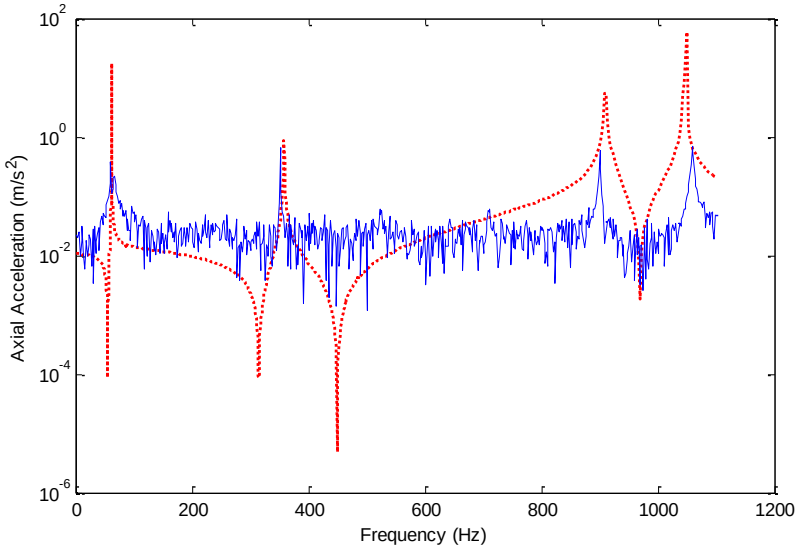

Fig.12 Axial acceleration of empty T-shaped pipe with axial impact: measurement (solid) and simulation results (dot).

The T-shaped pipe with oil was then tested with axial excitation, in the same way as was done by Vardy and Tijsseling *et al*. [53,54]. The pressure of the fluid inside was raised to 9.4 bar. Experimental results of fluid pressure as well as axial acceleration are shown in Fig.13, compared with simulation results. There is good agreement in the peaks at 58, 325, 371 and 1003 Hz on simulation curve in Fig.13(a), but the other two peaks (763 and 873 Hz) show bad agreement with measurements. Moreover, many other peaks of experimental results, like peaks of 194, 461 and 538 Hz, can not be found in the simulation result. Note that 538 Hz is actually a lateral mode. The measurements of fluid pressure at end C and axial acceleration show similar results.

The reason for the poor agreement is probably because the system is extremely sensitive to symmetry. It is not easy to build a completely symmetrical system; more importantly, neither does the steel rod hit along the centre axis precisely each time. The agreement is worse when the pipes are filled with oil because the FSI effect becomes significant.

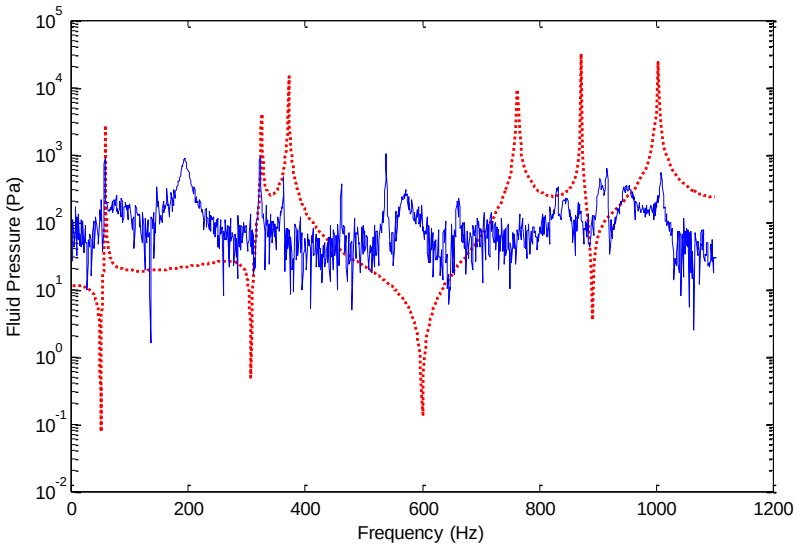

(a)

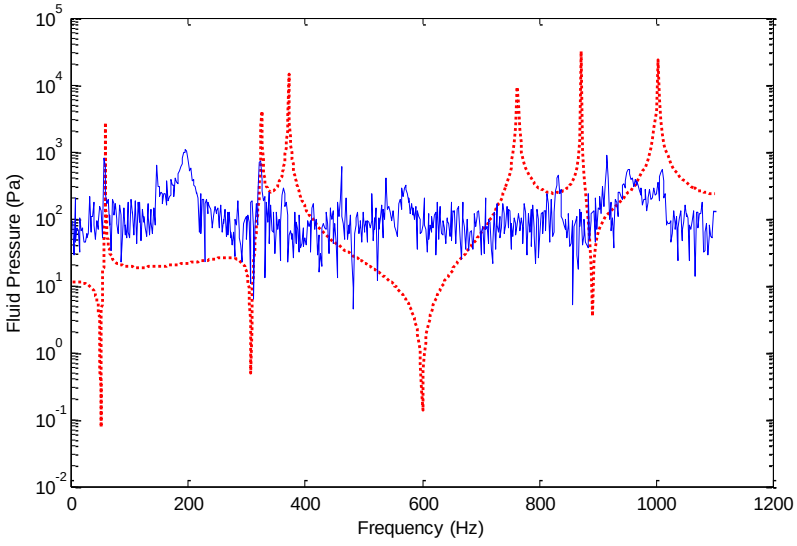

(b)

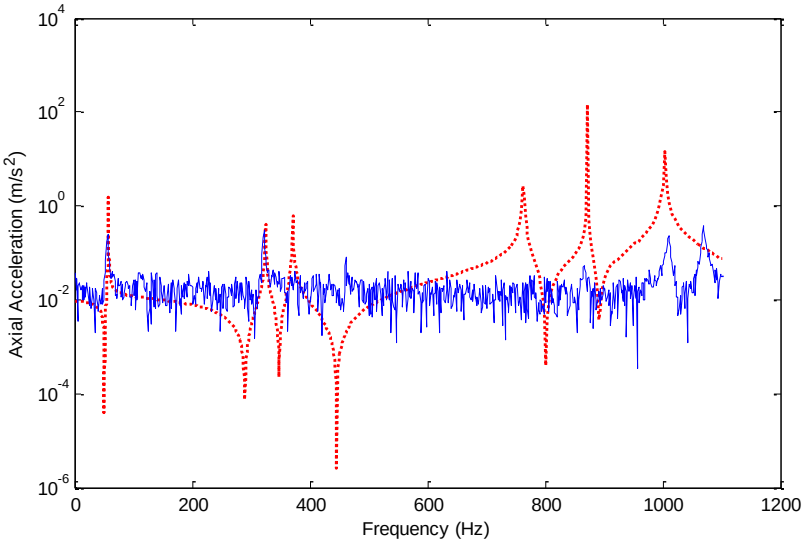

(c)

Fig.13 Frequency responses of T-shaped pipe with axial impact: measurement (solid)

and simulation results (dot). (a) Fluid pressure at end B; (b) Fluid pressure at end C; (c) Axial acceleration at T-piece.

Provided that one hits the pipe end laterally, lateral vibration can be induced by line impact between the rod's flat plane and circular pipe wall, without bringing in axial modes. Accordingly, a test with lateral excitation was used to avoid the problem of sensitivity to symmetry, and the initial pressure of the system was 9.4 bar. Exciting the system with lateral impact at pipe end A, the boundary and constraint matrix is the same as those in axial case, while the excitation vector at A would be written as

$$\mathbf{Q}_{\mathbf{A}}(\mathrm{s}) = \begin{bmatrix} 0 & 0 & (F_{rod}/\mathrm{s})(1-\mathrm{e}^{-\mathrm{s}T}) & 0 & 0 & 0 & 0 \end{bmatrix}^{\mathrm{T}}. \tag{41}$$

In Fig.14, the frequency spectrum of fluid pressure is compared with numerical simulation results, showing a much better agreement. Moreover, system natural frequencies from experiment and calculation are listed in Table 3. Compared with measurement results, simulation of the presented method achieves a good prediction with an average error of 1.0% in the natural frequencies. Small errors may be caused by the simplified model of compression type coupling, consisting of washer, O ring and screwed components, which would definitely affect the system's stiffness and damping. A simpler model, treating all fittings as lumped mass and neglecting their dimensions, gives out a less accurate prediction (Table 3, denoted as "previous method"). It is clear that one cannot simply neglect the effect of the T-piece fitting when the size of it is significant relative to the pipe lengths.

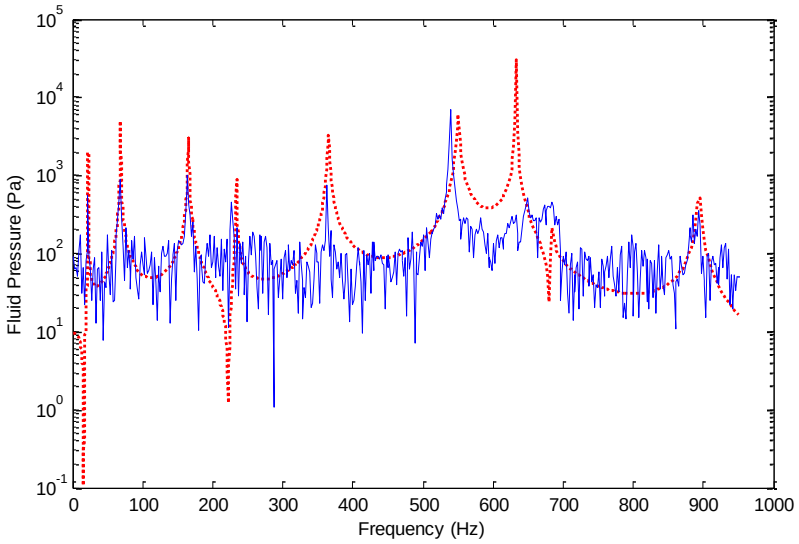

Fig.14 Fluid pressure at end B of T-shaped pipe with lateral impact: measurement (solid) and simulation results (dot).

Table 3 Natural frequencies of T-shaped pipe system with lateral excitation.

Measurement (Hz)	Simulation of presented method		Simulation of previous method	
	Frequency (Hz)	Error (%)	Frequency (Hz)	Error (%)
22.2	22.3	0.45	23.5	5.86
68.4	68.4	0.00	69.0	0.88

164.6	165.5	0.55	176.5	7.23
227.4	233.8	2.81	254.3	11.83
362.4	365.6	0.88	369.6	1.99
539.9	550.3	1.93	586.8	8.69
649.0	633.0	2.47	688.5	6.09
684.2	683.5	0.10	760.8	11.20
893.1	894.4	0.15	902.9	1.10

It is evident that solution of FSI in a T-junction system and the method of constraints are effective. Compression type couplings and dimensions of fittings were found to affect the system's characteristics significantly, so there is a need to use a relatively specific model to describe the T-piece fitting. The system excited by an axial impact was very sensitive to symmetry, which is mostly caused by imperfect axial excitation and would lead to a variability of frequency response. There was less variability in the case of lateral excitation.

4.2. Two-branch pipe

The configuration of a two-branch pipe assembly has not been investigated or carried out by previous work, though it is common in actual piping systems. The aim of this experiment was to validate the general solution of multi-branch pipes presented in the current paper. The two-branch pipe shown in Fig.15 consists of two T-piece fittings and five straight sections sealed with screwed taps. The rod to excite the system was hung by strings. The valve mentioned in the T-shaped pipe system was fitted in one of T-pieces for retaining fluid pressure. Pressure transducers were employed to measure the fluid pulsations, labelled by 'pt' in Fig.15.

Using the same method as for modelling of a T-shaped pipe, the T-piece fitting could be modelled as three thick straight sections with lumped mass. The configuration for calculation is depicted by node diagram in Fig.15 and mentioned in Table 4. The mass of a single T-piece was 1.36 kg, and the lumped mass at node 4 would be 0.12 kg. As for the T-piece with valve, which was the same as that in T-shaped pipe system, the lumped mass at node 10 was 0.32 kg. The mass of pressure transducer was negligible (0.01 kg) in the calculation. The fluid pressure in this experiment was 10 bar.

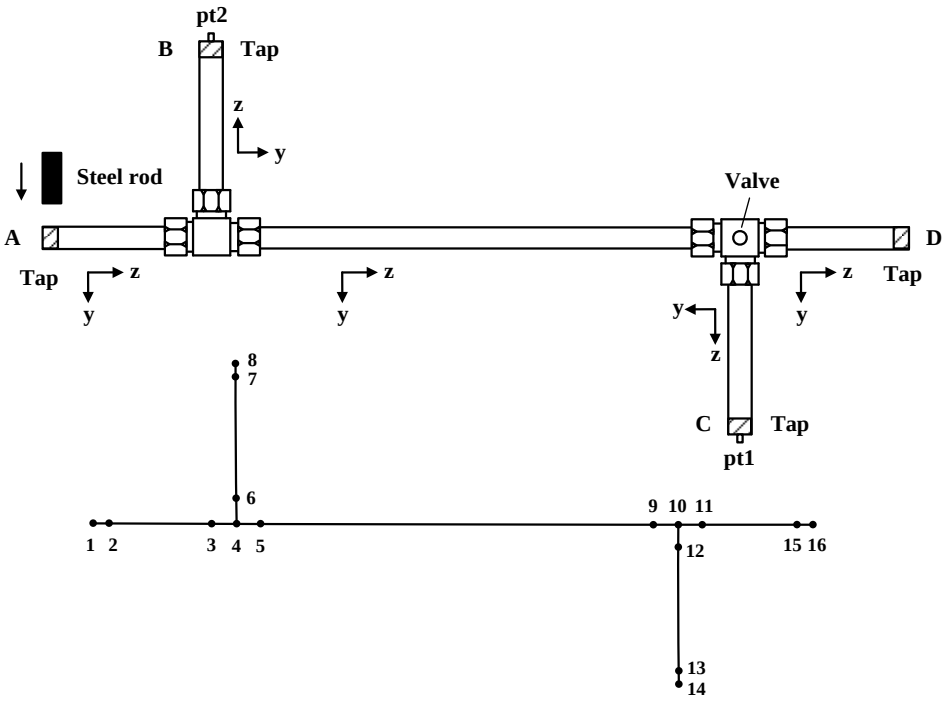

Fig.15 Schematic drawing of two-branch pipe system.
(pt = pressure transducer, Tap = tapped fitting)

Table 4 Dimensions of two-branch pipe.

Position	*Length (mm)*	*Inner/outer radii (mm)*	*Material*
1-2, 7-8, 13-14, 15-16	10	0.0 / 12.7	Steel
3-4, 4-5, 4-6,9-10,10-11,10-12	40	10.5 / 23.0	Steel
5-9	1142	10.5 / 12.7	Tungum
2-3,11-15	324	10.5 / 12.7	Tungum
6-7, 12-13	524	10.5 / 12.7	Tungum

For the same lateral impact force imposed on the pipe end as in the T pipe system, the excitation vector at position A is $-\mathbf{Q}_A$ given by Eq.(41), due to the different direction of local coordinate systems. Considering coordinate systems defined in Fig.C.1 in Appendix C, one can obtain that the boundary matrix at end A is $\mathbf{D}_0$ in Eq.(16), and matrices at position B, C and D are $\mathbf{D}_L$. Then the system could be calculated by the general method of multi-branch pipes in section 3.2 or the specific one mentioned in Appendix C.

The experimental result of fluid vibration is shown in Fig.16, compared with calculation using the presented method. Natural frequencies of measured and calculated results are listed specifically in Table 5, indicating good agreement with an average deviation of 2.3%. Amplitudes of some peaks (250.7, 267.6 and 577.3 Hz) on the calculation curve are very different from those of measurements, though frequencies match measurements closely. Most natural frequencies in the simulation are slightly larger than those measured in experiment. The reason may be that the reduction of stiffness, caused by compression type couplings, may become more significant when more T-pieces are assembled, but the T-piece model used in

simulation does not reflect this complex effect comprehensively. Nevertheless, the accuracy of prediction is sufficient and acceptable.

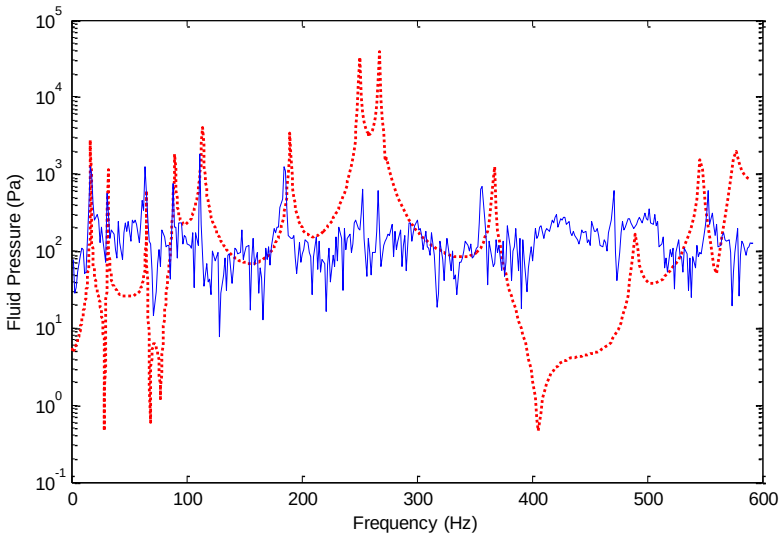

Fig.16 Frequency response of fluid pressure at end C in two-branch pipe with lateral impact: measurement (solid) and simulation results (dot).

Table 5 Natural frequencies of two-branch pipe system with lateral excitation.

Measurement (Hz)	Simulation of presented method (Hz)	Error (%)
16.1	17.0	5.59
30.7	31.7	3.26
64.4	65.2	1.24
87.8	90.0	2.51
111.2	113.7	2.25
184.4	189.9	2.98
253.2	250.7	0.99
266.4	267.6	0.45
357.1	367.5	2.91
471.3	489.5	3.86
553.3	545.6	1.39
578.2	577.3	0.16

When the impact was applied axially the agreement was poor, because the results are then very sensitive to impact misalignment or system asymmetry, as was found for the T-shaped pipe (section 4.1). Results are not shown here.

In this experiment, the general solution of a multi-branch pipe was applied on a two-branch case and shown to be correct.

5. Conclusion

The vibration response of piping systems with complex constraints, boundary conditions and spatial configurations are studied in this paper. The following conclusions can be drawn.

1. The frequency solution method of liquid-filled pipe systems based on fourteen-equation models has been developed. Various boundary conditions and complex structural constraints at both the end and the intermediate position are contained in this FSI solution.

2. A general solution of the multi-branch pipe is proposed, which is extended from the basic model of T-junction. This may offer a methodology to solve the complex hydraulic piping system with diverse fluid and structural excitation, while complex constraints are considered.

3. Two experiments of hung pipes made of hydraulic components with instantaneous impact were carried out to prove the methods presented in this work. The pipe assembly was suspended freely from strings and no pipe clamps were used. The method of constraints was used to model the mass of the pipe fittings. The results for the T-shaped pipe system validate the method of constraints, and reveal the necessity to build a specific model of the T-piece in the system with appropriate geometry and mass. Actual piping systems commonly contain multiple branches; the general solution of a multi-branch system has been validated by investigation of a two-branch pipe. This validates the general solution of multi-branch systems, which are common in actual piping systems. The experimental results match simulation well, indicating that the methods presented here are correct and effective. Although experiments in this work exclude damping and elastic constraints, the general method of constraints can be validated by considering mass only. However some variability was observed in the measurements especially when applying excitation in an axial direction because of the difficulty in ensuring a perfect axial excitation, such that some asymmetric and lateral modes may have been excited.

Further work might involve an investigation of the use of pipe clamps and supports using the method of constraints.

Acknowledgement

The authors express their gratitude to the National Basic Research Program of China (973 Program, 2014CB046405), National Nature Science Foundation of China (51235002), International Science & Technology Cooperation Program of China (2011DFA72690) and China Scholarship Council for the financial support of this research. The experimental work was supported by the UK Engineering and Physical Sciences Research Council under grant number EP/H024190/1. Contributions to the experiments by Alan Jefferis, Vijay Rajput and other technicians in Department of Mechanical Engineering at University of Bath are gratefully acknowledged. The reviewers are thanked for their valuable suggestions for improving the paper.

Appendix A: Fundamental equations of FSI in straight section

The fourteen fundamental equations for a straight pipe section (see Fig.2) are presented below, mostly based on the model developed by Lesmez and Wiggert *et al*. [21].

$$\frac{\partial V}{\partial t}+\frac{1}{\rho_f}\frac{\partial P}{\partial z}=0 \tag{A.1}$$

$$\frac{\partial V}{\partial z}+\frac{1}{K^*}\frac{\partial P}{\partial t}-2\nu\frac{\partial \dot{u}_z}{\partial z}=0\,,\quad \frac{1}{K^*}=\frac{1}{K}+(1-\nu^2)\frac{2r}{Ee} \tag{A.2}$$

$$\frac{\partial f_z}{\partial z}-A_p\rho_p\frac{\partial \dot{u}_z}{\partial t}=0 \tag{A.3}$$

$$\frac{\partial f_z}{\partial t}-A_p\nu\frac{r}{e}\frac{\partial P}{\partial t}-EA_p\frac{\partial \dot{u}_z}{\partial z}=0 \tag{A.4}$$

$$\frac{\partial f_y}{\partial z}-(\rho_f A_f+\rho_p A_p)\frac{\partial \dot{u}_y}{\partial t}=0 \tag{A.5}$$

$$\frac{\partial f_y}{\partial t}-\kappa^2 GA_p(\frac{\partial \dot{u}_y}{\partial z}+\dot{\psi}_x)=0\,,\quad \kappa^2=2\frac{1+\nu}{4+3\nu} \tag{A.6}$$

$$\frac{\partial m_x}{\partial z}-(\rho_p I_p+\rho_f I_f)\frac{\partial \dot{\psi}_x}{\partial t}-f_y=0 \tag{A.7}$$

$$\frac{\partial m_x}{\partial t}-EI_p\frac{\partial \dot{\psi}_x}{\partial z}=0 \tag{A.8}$$

$$\frac{\partial f_x}{\partial z}-(\rho_f A_f+\rho_p A_p)\frac{\partial \dot{u}_x}{\partial t}=0 \tag{A.9}$$

$$\frac{\partial f_x}{\partial t}-\kappa^2 GA_p(\frac{\partial \dot{u}_x}{\partial z}-\dot{\psi}_y)=0\,,\quad \kappa^2=2\frac{1+\nu}{4+3\nu} \tag{A.10}$$

$$\frac{\partial m_y}{\partial z}-(\rho_p I_p+\rho_f I_f)\frac{\partial \dot{\psi}_y}{\partial t}+f_x=0 \tag{A.11}$$

$$\frac{\partial m_y}{\partial t}-EI_p\frac{\partial \dot{\psi}_y}{\partial z}=0 \tag{A.12}$$

$$\frac{\partial m_z}{\partial z}-\rho_p J_p\frac{\partial \dot{\psi}_z}{\partial t}=0 \tag{A.13}$$

$$\frac{\partial m_z}{\partial t}-GJ_p\frac{\partial \dot{\psi}_z}{\partial z}=0 \tag{A.14}$$

Appendix B: Fundamental equations of FSI in T-junction

The method presented here is to describe the T-junction (Fig.6) just considering kinematic motion. The equations are based on the model in Ref. [56], and differences between these two models are due to differences in coordinate systems.

$$\{A_f(V-\dot{u}_z)\}_c=\{A_f(V-\dot{u}_z)\}_a-\{A_f(V-\dot{u}_z)\}_b \tag{B.1}$$

$$\{P\}_c=\{P\}_a=\{P\}_b \tag{B.2}$$

$$\{\dot{u}_z\}_c=\{\dot{u}_z\}_a=\{\dot{u}_y\}_b \tag{B.3}$$

$$\{f_z-A_fP\}_c=\{f_z-A_fP\}_a-\{f_y\}_b \tag{B.4}$$

$$\{\dot{u}_y\}_c=\{\dot{u}_y\}_a=-\{\dot{u}_z\}_b \tag{B.5}$$

$$\{f_y\}_c=\{f_y\}_a+\{f_z-A_fP\}_b \tag{B.6}$$

$$\{\dot{\psi}_x\}_c=\{\dot{\psi}_x\}_a=\{\dot{\psi}_x\}_b \tag{B.7}$$

$$\{m_x\}_c=\{m_x\}_a-\{m_x\}_b \tag{B.8}$$

$$\{\dot{u}_x\}_c=\{\dot{u}_x\}_a=\{\dot{u}_x\}_b \tag{B.9}$$

$$\{f_x\}_c=\{f_x\}_a-\{f_x\}_b \tag{B.10}$$

$$\{\dot{\psi}_y\}_c=\{\dot{\psi}_y\}_a=-\{\dot{\psi}_z\}_b \tag{B.11}$$

$$\{m_y\}_c=\{m_y\}_a+\{m_z\}_b \tag{B.12}$$

$$\{\dot{\psi}_z\}_c=\{\dot{\psi}_z\}_a=\{\dot{\psi}_y\}_b \tag{B.13}$$

$$\{m_z\}_c=\{m_z\}_a-\{m_y\}_b \tag{B.14}$$

Appendix C: Solution method of two-branch pipeline

Coordinate systems of the 2-branch piping system are depicted in Fig.C.1, which could be considered as a pipe system with a series of two T-junctions. $\tilde{\boldsymbol{\phi}}_1(0,\mathrm{s})$, $\tilde{\boldsymbol{\phi}}_2(L_2,\mathrm{s})$, $\tilde{\boldsymbol{\phi}}_4(L_4,\mathrm{s})$ and $\tilde{\boldsymbol{\phi}}_5(L_5,\mathrm{s})$ are state vectors at four pipe ends, in which L_i $(1\le i\le 5)$ is the length of pipe i shown in Fig.C.1.

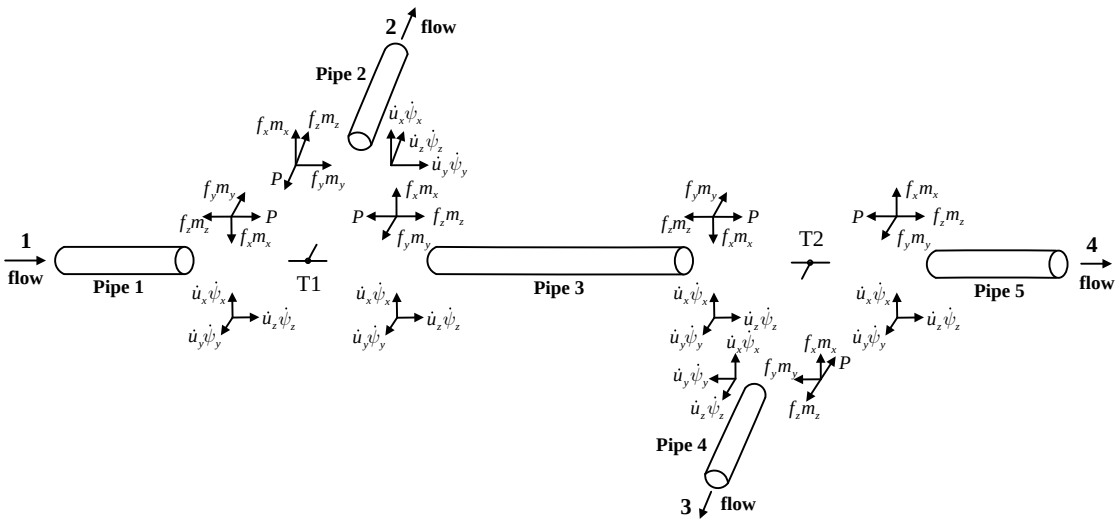

Fig.C.1 Schematic diagram of T-junction nodes in two-branch pipeline.

The relation of state vectors at three ports of the left T-junction node is

$$\begin{pmatrix} \tilde{\boldsymbol{\phi}}_3(0,\mathrm{s}) \\ \mathbf{0} \end{pmatrix}_{21\times1} = \mathbf{T}_1(\mathrm{s}) \begin{pmatrix} \mathbf{M}_1(L_1,\mathrm{s})\tilde{\boldsymbol{\phi}}_1(0,\mathrm{s}) \\ \mathbf{M}_2^{-1}(L_2,\mathrm{s})\tilde{\boldsymbol{\phi}}_2(L_2,\mathrm{s}) \end{pmatrix}_{28\times1}, \tag{C.1}$$

in which $\mathbf{M}_1$ and $\mathbf{M}_2$ is the field transfer matrix of pipe 1 and pipe 2 respectively, and $\mathbf{T}_1$ is the point transfer matrix of this T-junction node. Then the state vector at the right end of pipe 3 can be expressed as

$$\begin{pmatrix} \tilde{\boldsymbol{\phi}}_3(L_3,\mathrm{s}) \\ \mathbf{0} \end{pmatrix}_{21\times1} = \mathbf{G}_1(\mathrm{s})\mathbf{T}_1(\mathrm{s})\mathbf{J} \begin{pmatrix} \mathbf{M}_2^{-1}(L_2,\mathrm{s})\tilde{\boldsymbol{\phi}}_2(L_2,\mathrm{s}) \\ \mathbf{M}_1(L_1,\mathrm{s})\tilde{\boldsymbol{\phi}}_1(0,\mathrm{s}) \end{pmatrix}_{28\times1}, \tag{C.2}$$

where

$$\mathbf{G}_1(\mathrm{s}) = \begin{pmatrix} \mathbf{M}_3(L_3,\mathrm{s}) & \mathbf{0} \\ \mathbf{0} & \mathbf{I}_{7\times7} \end{pmatrix}_{21\times21} \text{ and } \mathbf{J} = \begin{pmatrix} \mathbf{0} & \mathbf{I}_{14\times14} \\ \mathbf{I}_{14\times14} & \mathbf{0} \end{pmatrix}. \tag{C.3}$$

The relation at the right T-junction node would be

$$\begin{pmatrix} \tilde{\boldsymbol{\phi}}_5(0,\mathrm{s}) \\ \mathbf{0} \end{pmatrix}_{21\times1} = \mathbf{T}_2(\mathrm{s}) \begin{pmatrix} \tilde{\boldsymbol{\phi}}_3(L_3,\mathrm{s}) \\ \mathbf{M}_4^{-1}(L_4,\mathrm{s})\tilde{\boldsymbol{\phi}}_4(L_4,\mathrm{s}) \end{pmatrix}_{28\times1}, \tag{C.4}$$

which can also be written as

$$\begin{pmatrix} \tilde{\boldsymbol{\phi}}_5(L_5,\mathrm{s}) \\ \mathbf{0} \end{pmatrix}_{28\times1} = \mathbf{F}_2(\mathrm{s}) \begin{pmatrix} \mathbf{M}_4^{-1}(L_4,\mathrm{s})\tilde{\boldsymbol{\phi}}_4(L_4,\mathrm{s}) \\ \tilde{\boldsymbol{\phi}}_3(L_3,\mathrm{s}) \\ \mathbf{0} \end{pmatrix}_{35\times1}, \tag{C.5}$$

where

$$\mathbf{F}_2(\mathrm{s}) = \begin{pmatrix} \mathbf{G}_2(\mathrm{s})\mathbf{T}_2(\mathrm{s})\mathbf{J} & \mathbf{0} \\ \mathbf{0} & \mathbf{I}_{7\times7} \end{pmatrix}_{28\times35} \text{ and } \mathbf{G}_2(\mathrm{s}) = \begin{pmatrix} \mathbf{M}_5(L_5,\mathrm{s}) & \mathbf{0} \\ \mathbf{0} & \mathbf{I}_{7\times7} \end{pmatrix}_{21\times21}. \tag{C.6}$$

Relating to Eq.(C.2), Eq.(C.5) can be written as

$$\begin{pmatrix} \tilde{\boldsymbol{\phi}}_5(L_5,\mathrm{s}) \\ \mathbf{0} \end{pmatrix}_{28\times 1} = \mathbf{F}_2(\mathrm{s})\mathbf{F}_1(\mathrm{s})\mathbf{L}\begin{pmatrix} \mathbf{M}_1(L_1,\mathrm{s})\tilde{\boldsymbol{\phi}}_1(0,\mathrm{s}) \\ \mathbf{M}_2^{-1}(L_2,\mathrm{s})\tilde{\boldsymbol{\phi}}_2(L_2,\mathrm{s}) \\ \mathbf{M}_4^{-1}(L_4,\mathrm{s})\tilde{\boldsymbol{\phi}}_4(L_4,\mathrm{s}) \end{pmatrix}_{42\times 1}, \tag{C.7}$$

where

$$\mathbf{F}_1(\mathrm{s}) = \begin{pmatrix} \mathbf{I}_{14\times 14} & \mathbf{0} \\ \mathbf{0} & \mathbf{G}_1(\mathrm{s})\mathbf{T}_1(\mathrm{s})\mathbf{J} \end{pmatrix}_{35\times 42} \text{ and } \mathbf{L} = \begin{pmatrix} & & \mathbf{I}_{14\times 14} \\ & \mathbf{I}_{14\times 14} & \\ \mathbf{I}_{14\times 14} & & \end{pmatrix}. \tag{C.8}$$

For the boundary equation for this system is

$$\begin{pmatrix} \mathbf{D}_1(\mathrm{s})\tilde{\boldsymbol{\phi}}_1(0,\mathrm{s}) \\ \mathbf{D}_2(\mathrm{s})\tilde{\boldsymbol{\phi}}_2(L_2,\mathrm{s}) \\ \mathbf{D}_3(\mathrm{s})\tilde{\boldsymbol{\phi}}_4(L_4,\mathrm{s}) \\ \mathbf{D}_4(\mathrm{s})\tilde{\boldsymbol{\phi}}_5(L_5,\mathrm{s}) \end{pmatrix} = \begin{pmatrix} \mathbf{Q}_1(\mathrm{s}) \\ \mathbf{Q}_2(\mathrm{s}) \\ \mathbf{Q}_3(\mathrm{s}) \\ \mathbf{Q}_4(\mathrm{s}) \end{pmatrix}, \tag{C.9}$$

Hence, one can obtain the solution equation as below,

$$\begin{pmatrix} \mathbf{D}_1(\mathrm{s}) & & & \\ & \mathbf{D}_2(\mathrm{s}) & & \\ & & \mathbf{D}_3(\mathrm{s}) & \\ \mathbf{H}(\mathrm{s})\mathbf{F}_2(\mathrm{s})\mathbf{F}_1(\mathrm{s})\mathbf{L}\mathbf{M}_\mathbf{T}(\mathrm{s}) & & & \end{pmatrix}_{42\times 42} \begin{pmatrix} \tilde{\boldsymbol{\phi}}_1(0,\mathrm{s}) \\ \tilde{\boldsymbol{\phi}}_2(L_2,\mathrm{s}) \\ \tilde{\boldsymbol{\phi}}_4(L_4,\mathrm{s}) \end{pmatrix}_{42\times 1} = \begin{pmatrix} \mathbf{Q}_1(\mathrm{s}) \\ \mathbf{Q}_2(\mathrm{s}) \\ \mathbf{Q}_3(\mathrm{s}) \\ \mathbf{Q}_4(\mathrm{s}) \\ \mathbf{0} \end{pmatrix}_{42\times 1}. \tag{C.10}$$

where

$$\mathbf{H}(\mathrm{s}) = \begin{pmatrix} \mathbf{D}_4(\mathrm{s}) & \mathbf{0} \\ \mathbf{0} & \mathbf{I}_{14\times 14} \end{pmatrix}_{21\times 28}, \tag{C.11}$$

$$\mathbf{M}_\mathbf{T}(\mathrm{s}) = \begin{pmatrix} \mathbf{M}_1(L_1,\mathrm{s}) & & \\ & \mathbf{M}_2^{-1}(L_2,\mathrm{s}) & \\ & & \mathbf{M}_4^{-1}(L_4,\mathrm{s}) \end{pmatrix}_{42\times 42}. \tag{C.12}$$

Thus, the state vector at port 4 can be calculated by

$$\tilde{\boldsymbol{\phi}}_5(L_5,\mathrm{s}) = \begin{matrix} \mathbf{I}_{14\times 14} & \mathbf{0}_{14\times 28} \end{matrix} \mathbf{F}_2(\mathrm{s})\mathbf{F}_1(\mathrm{s})\mathbf{L}\mathbf{M}_\mathbf{T}(\mathrm{s}) \begin{pmatrix} \tilde{\boldsymbol{\phi}}_1(0,\mathrm{s}) \\ \tilde{\boldsymbol{\phi}}_2(L_2,\mathrm{s}) \\ \tilde{\boldsymbol{\phi}}_4(L_4,\mathrm{s}) \end{pmatrix}_{42\times 1}. \tag{C.13}$$

If constraints at T-junction node are considered, one should modify the transfer matrix of any pipe section connecting to the junction by simply multiplying the constraint matrix, which is mentioned in section 3.1 specifically.

References

[1] N. Joukowsky, On the hydraulic hammer in water supply pipes, 1898, English translation by O. Simin: *Waterhammer. International Proceedings of the 24th Annual Convention of the American Water Works Association*, St. Louis, USA., June 1904, pp.341-424.

[2] A.S. Tijsseling, Fluid-structure interaction in liquid-filled pipe systems: a review, *Journal of Fluids and Structures*, 10, 1996, pp.109-146.

[3] E.B. Wylie, V.L. Streeter, *Fluid transients*, McGraw-Hill, New York, 1978.

[4] Y. Cai, Dynamics of fluid-conveying pipes, Zhejiang University Press, Hangzhou, China, 1990. (in Chinese)

[5] D.C. Wiggert, A.S. Tijsseling, Fluid transients and fluid-structure interaction in flexible liquid-filled piping, *ASME Applied Mechanics Reviews*, 54(5), 2001, pp.455-481.

[6] L. Zhang, A.S. Tijsseling, A.E. Vardy, FSI analysis of liquid-filled pipes, *Journal of Sound and Vibration*, 224(1), 1999, pp.69-99.

[7] M. Zielke, Frequency dependent friction in transient pipe flow, PhD thesis, Department of Civil Engineering, University of Michigan, 1966.

[8] R. Skalak, An extension of the theory of water hammer, *Transaction of the ASME*, 78(1), 1956, pp.105-116.

[9] A.S. Tijsseling, M.F. Lambert, A.R. Simpson, M.L. Stephens, J.P. Vítkovský, A. Bergant, Skalak's extended theory of water hammer. *Journal of Sound and Vibration*, 310(3), 2008, pp. 718-728.

[10] D.C. Wiggert, R.S. Otwell, F.J. Hatfield, The effect of elbow restraint on pressure transients, *ASME Journal of Fluids Engineering*, 107(3), 1985, pp.402-406.

[11] J.S. Walker, J.W., Phillips, Pulse propagation in fluid-filled tubes, *ASME Journal of Applied Mechanics*, 44, 1977, pp.31-35.

[12] D.D. Budny, D.C. Wiggert, F.J. Hatfield, The influence of structural damping on internal pressure during a transient pipe flow, *ASME Journal of Fluids Engineering*, 113(3), 1991, pp. 424-429.

[13] A.S. Tijsseling, Exact solution of linear hyperbolic four-equation system in axial liquid-pipe vibration, *Journal of Fluids and Structures*, 18, 2003, pp.179-196.

[14]A.S. Tijsseling, Exact computation of the axial vibration of two coupled liquid-filled pipes. *Proceedings of the ASME 2009 Pressure Vessels and Piping Division Conference*, Prague, Czech Republic, July 2009, Paper PVP2009-77250.

[15] L.C. Davidson, J.E. Smith, Liquid-structure coupling in curved pipes, *Shock and Vibration Bulletin*, 40, Part 4, 1969, pp.197-207.

[16] R.A. Valentin, J.W. Phillips, J.S. Walker, Reflection and transmission of fluid transients at an elbow, *5th SMiRT Conference*, Berlin, Germany, Paper B, Aug 1979, pp.2-6.

[17] C.K. Hu, J.W. Phillips, Pulse propagation in fluid-filled elastic curved tubes, *ASME Journal of Pressure Vessel Technology*, 103(1), 1981, pp.43-49.

[18] L.C. Davidson, D.R. Samsury, Liquid-structure coupling in curved pipes – II, *The shock and Vibration Bulletin*, 42, Part 1, 1972, pp.123-136.

[19] D.H. Wilkinson, Acoustic and mechanical vibrations in liquid-filled pipework systems, *Proceedings of the BNES International Conference on Vibration in Nuclear Plant*, Keswick, UK, May 1978, pp.863-878.

[20] D.C. Wiggert, F.J. Hatfield, S. Stuckenbruck, Analysis of liquid and structural transients in piping by the method of characteristics, *ASME Journal of Fluids Engineering*, 109, 1987, pp.161-165.

[21] M.W. Lesmez, D.C. Wiggert, F.J. Hatfield, Modal analysis of vibrations in liquid-filled piping systems, *ASME Journal of Fluids Engineering*, 112(3), 1990, pp.311-318.

[22] M.W. Lesmez, Modal analysis of vibration in liquid-filled piping systems, PhD thesis, Department of Civil and Environment Engineering, Michigan State University, USA, 1989.

[23] S.C. Tentarelli, Propagation of noise and vibration in complex hydraulic tubing systems, PhD thesis, Department of Mechanical Engineering, Lehigh University, USA, 1990.
[24] M. El-Raheb, Vibrations of three-dimensional pipe systems with acoustic coupling, *Journal of sound and vibration*, 78(1), 1981, pp.39-67.
[25] C.A.F. De Jong, Analysis of pulsations and vibrations in fluid-filled pipe systems, PhD thesis, Department of Mechanical Engineering, Eindhoven University of Technology, The Netherlands, 1994.
[26] A.H.M Kwong, K. A. Edge, Wave propagation in fluid-filled pipe system, *International Proceedings of Conference Euro-Noise '95*, Lyon, France, Vol.3, 1995, pp.745-750.
[27] A.H.M. Kwong, K.A. Edge, Structure-borne noise prediction in liquid-conveying pipe systems, *Proceedings of IMechE Part I: Journal of Systems and Control Engineering*, 210(3), 1996, pp.189-200.
[28] A.H.M. Kwong, K.A. Edge, A method to reduce noise in hydraulic systems by optimizing pipe clamp locations, *Proceedings of IMechE Part I: Journal of Systems and Control Engineering*, 212(4), 1998, pp.267-280.
[29] Z. Jiao, Q. Hua, K. Yu, Frequency domain analysis of vibrations in liquid-filled piping systems, *Acta Aeronautica et Astronautica Sinica*, 20(4), 1999, pp.316-320. (in Chinese).
[30] G. Liu, Y. Li, Vibration analysis of liquid-filled pipelines with elastic constraints, *Journal of Sound and Vibration*, 330(13), 2011, pp.3166-3181.
[31] E.C. Pestel, F.A. Leckie, *Matrix methods in elastomechanics*, McGraw-Hill, New York, 1963.
[32] M.H. Chaudhry, Resonance in pressurized piping systems, PhD thesis, Department of Civil Engineering, University of British Columbia, Canada, 1970.
[33] W. Burmann, Water hammer in coaxial pipe system, *Journal of Hydraulics Division*, 101(6), 1975, pp.699-715.
[34] W. Schwarz, Waterhammer calculations taking into account the radial and longitudinal displacements of the pipe wall, PhD thesis, University of Stuttgart, German, 1978.
[35] J. Ellis, A study of pipe-liquid interaction following pump trip and check-valve closure in a pumping station, *Proceedings 3rd International Conference on Pressure Surges*, Canterbury, England, Vol.1, Mar 1980, pp.203-220.
[36] A.S. Tijsseling, Fluid-structure interaction in case of waterhammer with cavitation, PhD thesis, Faculty of Civil Engineering, Delft University of Technology, The Netherlands, 1993.
[37] R.G. Da Rocha, F.B. De Freitas Rachid, Numerical solution of fluid-structure interaction in piping systems by Glimm's method, *Journal of Fluids and Structures*, 28, 2012, pp.392-415.
[38] C.S.W Lavooij, A.S. Tijsseling, Fluid-structure interaction in liquid-filled piping systems, *Journal of Fluids and Structures*, 5(5), 1991, pp.573-595.
[39] J. Gale, I. Tiselj, Godunov's method for simulations of fluid-structure interaction in piping systems, *ASME Journal of Pressure Vessel Technology*, 130(031304), 2008, pp.1-12.
[40] E. Kojima, M. Shinada, J. Yu, Development of accurate and practical simulation technique based on the modal approximations for fluid transients in compound fluid-line systems (1st report), *International Journal of Fluid Power*, 3(2), 2002, pp.5-15.
[41] A.F. D'Souza, R. Oldenburger, Dynamic response of fluid lines, *ASME Journal of Fluids Engineering*, 86(3), 1964, pp.589-598.
[42] S. Nanayakkara, N.D. Perreira, Wave propagation and attenuation in piping system, *ASME Journal of Vibration, Acoustics, Stress, and Reliability in Design*, 108(4), 1986, pp.441-446.
[43] Y. Li, G. Liu, J. Ma, Research on fluid-structure interaction in fluid-filled pipes, *Journal of Vibration and Shock*, 29(6), 2010, pp.50-53,124. (in Chinese)
[44] F.J. Hatfield, D.C. Wiggert, R.S. Otwell, Fluid structure interaction in piping by component synthesis, *ASME Journal of Fluids Engineering*, 104(3), 1982, pp.318-325.
[45] A.S. Tijsseling, A.E. Vardy, D. Fan, Fluid-structure interaction and cavitation in a single-elbow pipe system, *Journal of Fluids and Structures*, 10(4), 1996, 395-420.
[46] W. Borutzky, Bond graph modelling and simulation of multidisciplinary systems – An introduction, *Simulation Modelling Practice and Theory*, 17(1), 2009, pp.3-21.

[47] P.E. Wellstead, *Introduction to physical system modelling*, Original publisher: Academic Press Ltd, London, 1979, pp.177 (Electronic publisher: Control Systems Principles, 2000).
[48] D.D. Budny, D.C. Wiggert, F.J. Hatfield, The influence of structural damping on internal pressure during a transient pipe flow, Journal of Fluids Engineering, 113(3), 1991, pp.424-429.
[49] A.G.T.J. Heinsbroek, A.S. Tijsseling, The influence of support rigidity on waterhammer pressures and pipe stresses, *Proceedings of the 2nd International Conference on Water Pipeline Systems*, BHR Group, Edinburgh, UK, May 1994, pp.17-30.
[50] A.S. Tijsseling, A.E. Vardy, Axial modelling and testing of a pipe rack, *Proceedings of the 7th International Conference on Pressure Surges*, BHR Group, Harrogate, UK, April 1996, pp.363-383.
[51] J.S. Wu, P.Y. Shih, The dynamic analysis of a multispan fluid-conveying pipe subjected to external load, *Journal of Sound and Vibration*, 239(2), 2001, pp.201-215.
[52] K. Yang, Q.S. Li, L. Zhang, Longitudinal vibration analysis of multi-span liquid-filled pipelines with rigid constraints, *Journal of Sound and Vibration*, 273(1-2), 2004, pp.125-147.
[53] A.E. Vardy, D. Fan, A.S. Tijsseling, Fluid-structure interaction in a T-piece pipe, *Journal of Fluids and Structures*, 10(7), 1996, pp.763-786.
[54] A.S. Tijsseling, A.E. Vardy, Fluid-structure interaction and transient cavitation tests in a T-piece pipe, *Journal of Fluids and Structures*, 20(6), 2005, pp.753-762.
[55] A.S. Tijsseling, A.E. Vardy, Twenty years of FSI experiments in Dundee. *Proceedings of the Third M.I.T. Conference on Computational Fluid and Solid Mechanics (Editor K.J. Bathe)*, Elsevier, Boston, USA, June 2005, pp.1014-1017
[56] A.S. Tijsseling, P. Vaugrante, FSI in L-shaped and T-shaped pipe systems, *Proceedings of the 10th International Meeting of the IAHR Work Group on the Behaviour of Hydraulic Machinery under Steady Oscillatory Conditions*, Trondheim, Norway, 2001, Paper C3.